Institute for
Communications
and Navigation

Adaptive Kalman Filter-Based Phase-Tracking in GNSS

Mario Gómez Arias
Universitat Politècnica de Catalunya (UPC)

A Thesis submitted for the Degree of
Enginyeria Tècnica d'Aeronàutica, esp. en
Aeronavegació
(BSc in Air Navigation Systems and
Technologies)

Institute for Communications and Navigation

Prof. Dr. Christoph Günther

Supervised by Prof. Dr. C. Günther
Dipl.-Ing. K. Giger

July, 2010

Institute for Communications and Navigation

Technische Universität München
Theresienstrasse 90
80333 Munich

Abstract

This work introduces, implements and evaluates different adaptive Kalman filtering techniques based on the innovation autocorrelation function. The reason of considering these adaptive techniques is the effect of a wrong noise statistics initialization in a Kalman filter and the resulting estimation errors. Of course, different noise statistics than the actual for the stochastic process under estimation would lead to significant errors. For that reason, it is interesting to have a meaning of the effect of wrong noise statistics and to adapt these quantities when necessary.

The adaptive techniques considered within this work are the innovation autocorrelation based methods. The particularity of these methods is that the innovation sequence, defined as the new information introduced by the measurements, is a stationary Gaussian white noise sequence for an optimum filter. Moreover, an estimate of the autocorrelation function of that innovation sequence is obtained easily by using the ergodic property of a stationary sequence.

Finally, the Kalman filter is applied to the problem of carrier-phase tracking in a GNSS receiver. Some of the algorithms are evaluated for the case of carrier-phase tracking. Different scenarios from different measurement campaigns are used in this later implementation. The results demonstrate the estimated values of the noise variances for a carrier-phase tracking loop.

Zusammenfassung

Diese Arbeit beschreibt und evaluiert verschiedene adaptive Kalman Filter Verfahren, welche auf der Autokorrelationsfunktion der Innovationssequenz basieren. Die Motivation adaptive Techniken zu untersuchen, ist der Effekt eines suboptimal initialisierten Kalman Filters und den daraus resultierenden Schätzfehlern. Natürlich ergeben unterschiedliche Werte für die Rauschkovarianzmatrizen im Prozess und Schätzmodell signifikante Abweichungen. Deshalb ist es zuerst interessant die Bedeutung von falsch gewählten Statistiken zu kennen und diese Werte, wenn nötig, adaptiv anzupassen.
Die adaptiven Verfahren, welche in dieser Arbeit diskutiert werden, basieren auf der Korrelation der Innovationssequenz. Für ein optimales Filter kann gezeigt werden, dass diese Innovationssequenz, definiert als die neue Information eingeführt durch Messdaten, normalverteilt und weiss ist. Durch Ausnützen der Ergodizität einer stationären Sequenz, kann zudem eine Schätzung der Korrelationsfunktion der Innovationssequenz berechnet werden.
In dieser Arbeit wir der Kalman Filter zusätzlich für die Regelung der Trägerphase in einem GNSS Empfänger eingesetzt. Einige der diskutierten Algorithmen werden am Beispiel der Trägerphasen-Regelung getestet. Dazu werden Messdaten unterschiedlicher Messkampagnen verarbeitet. Die Resultate liefern einen Hinweis auf die Statistiken der Rauschprozesse im Trägerphasenregelkreis.

Contents

Chapter 1

Introduction

The main purpose of GNSS signal tracking is to achieve a fine synchronization between the receiver and the incoming signal for later processing stages such as the navigation message demodulation and the pseudorange/phase measurement. There exist different approaches in the problem of tracking. Despite the diversity of approaches and techniques involving tracking, this study is focused in those related with carrier-phase tracking. The interest in carrier-phase tracking is that it represents the weakest link at the receiver after acquisition and needs a particular processing.
The traditional carrier-phase tracking architecture consists of a first-, second- or third-order phase lock loop (PLL) filter and a proportional controller responsible for adjusting the locally generated signal copy to that received at the antenna. The carrier-phase steering of the local copy is achieved by means of a numerically controlled oscillator (NCO) and a discriminator provides a measure of the phase error between the signals. Figure 1.1 shows a typical carrier-phase tracking loop in a GNSS receiver. The relative simplicity of such a tracking architecture should be contrasted with its main limitation; a filter of this form assumes a deterministic signal dynamics model which is not the actual case.
The recent software-defined GNSS receivers and the increasing computing power of these receivers have made possible more robust and powerful tracking solu-

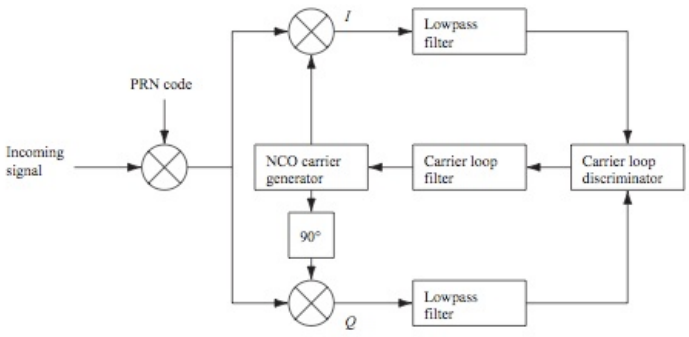

Figure 1.1: Typical carrier-phase tracking loop

tions to that discussed above. The Kalman filter-based tracking architecture is an example. The signal dynamics are modeled as a linear stochastic process and the problem of tracking turns mainly into an estimation problem.
In Chapter 2, several simulations were aimed to evaluate the performance of a Kalman filter for wrong parameter initialization, i.e., wrong noise statistics parameters and state vector dimension mismatch. Furthermore, large estimation errors appear when the performance of the Kalman filter is suboptimum. For that reason, it is necessary to apply some self-correcting technique when the performance of the Kalman filter is suboptimum, i.e., a method of adaptive filtering. The purpose of an adaptive filter is to reduce the large estimation errors due to wrong a priori noise statistics in a Kalman filter.
There exist different adaptive techniques. The multiple model adaptive estimation (MMAE) is composed of multiple elemental parallel Kalman filters, each using the same measurements but under different statistical filter matrices, i.e., the process and measurement noise covariance matrices $\mathbf{Q}$ and $\mathbf{R}$, respectively. The conditional probability associated to each estimate is obtained based on the measurements. Finally, the scheme forms the adaptive optimal estimate as a weighted sum of the estimates produced by each of the individual Kalman filters using that conditional probability. Figure 1.2 illustrates a MMAE scheme. For the problem of phase tracking, a MMAE scheme would imply to have a bank of filters for each satellite signal, resulting in a large quantity of filters. Therefore, that scheme has been not considered within this work. Other approaches

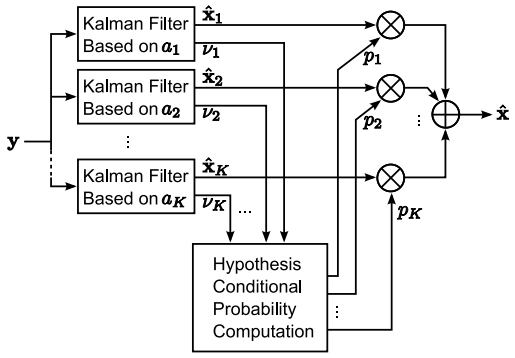

Figure 1.2: Multiple model adaptive estimation

in adaptive filtering are discussed in [1]. The innovation correlation adaptive methods are of particular interest as they make use of the zero-mean Gaussian white noise property of the innovation sequence defined as:

$$\boldsymbol{\nu}_k = \mathbf{y}_k - \mathbf{C}\hat{\mathbf{x}}_k^- \tag{1.1}$$

Some of these innovation correlation methods are discussed in Chapter 3.
Different adaptive algorithms were implemented and tested for a simulated stochastic process with different parameter initialization (see Chapter 3). The design parameters of some of the algorithms were also considered and evaluated. The results served as guidelines for the later implementation in a GNSS software-defined receiver in Chapter 5.

Chapter 2

Kalman Filter Performance For Wrong Parameter Initialization

2.1 Discrete-time system (signal) dynamics and Kalman filter form

The discrete-time signal dynamics model considered in this evaluation of the Kalman filter performance is described by the equations:

$$\mathbf{x}_{k+1} = \mathbf{A}\mathbf{x}_k + \mathbf{w}_k \tag{2.1}$$

$$\mathbf{y}_k = \mathbf{C}\mathbf{x}_k + \mathbf{v}_k \tag{2.2}$$

where $\mathbf{x}_k$ is the n-dimensional state vector, $\mathbf{A}$ is the state transition matrix, $\mathbf{w}_k$ is the process noise vector, $\mathbf{y}_k$ is the p-dimensional measurement vector, $\mathbf{C}$ is the observation mapping matrix, and $\mathbf{v}_k$ is the measurement noise vector. The sequences $\mathbf{v}_k$ and $\mathbf{w}_k$ are uncorrelated Gaussian white noise sequences with the properties:

$$\mathbb{E}\{\mathbf{v}_i\} = 0, \quad \mathbb{E}\left\{\mathbf{v}_i {\mathbf{v}_j}^T\right\} = \mathbf{R}\delta_{ij} \tag{2.3}$$

$$\mathbb{E}\{\mathbf{w}_i\} = 0, \quad \mathbb{E}\left\{\mathbf{w}_i {\mathbf{w}_j}^T\right\} = \mathbf{Q}\delta_{ij} \tag{2.4}$$

$$\mathbb{E}\left\{\mathbf{v}_i {\mathbf{w}_j}^T\right\} = \mathbf{0}_{pxn}, \quad \text{for any } i \text{ and } j \tag{2.5}$$

where $\mathbf{Q}$ and $\mathbf{R}$ are the process and measurement noise covariance matrices, respectively, $\mathbf{0}_{pxn}$ denotes the pxn zero matrix, and δ_{ij} is the Kronecker's delta defined as:

$$\delta_{ij} = \begin{cases} 1 & \text{if } i = j, \\ 0 & \text{if } i \neq j \end{cases} \tag{2.6}$$

The derivation of the particular matrix expressions used in this evaluation of the Kalman filter is left for Appendix A.

Given an initial *a priori* estimate of the state $\hat{\mathbf{x}}_0$ and its state error covariance $\hat{\mathbf{P}}_0$, the optimum linear unbiased estimate for the system defined by (2.1) and (2.2) is:

$$\begin{aligned}
\text{State propagation:} \quad \hat{\mathbf{x}}_k^- &= \mathbf{A}\hat{\mathbf{x}}_{k-1} && (2.7)\\
\hat{\mathbf{P}}_k^- &= \mathbf{A}\hat{\mathbf{P}}_{k-1}\mathbf{A}^T + \hat{\mathbf{Q}} && (2.8)\\
\text{Kalman gain:} \quad \mathbf{K}_k &= \hat{\mathbf{P}}_k^-\mathbf{C}^T\left[\mathbf{C}\hat{\mathbf{P}}_k^-\mathbf{C}^T + \hat{\mathbf{R}}\right]^{-1} && (2.9)\\
\text{State estimation:} \quad \hat{\mathbf{x}}_k &= \hat{\mathbf{x}}_k^- + \mathbf{K}_k\boldsymbol{\nu}_k && (2.10)\\
\hat{\mathbf{P}}_k &= (\mathbf{I} - \mathbf{K}_k\mathbf{C})\,\hat{\mathbf{P}}_k^- && (2.11)\\
\text{Innovation sequence:} \quad \boldsymbol{\nu}_k &= \mathbf{y}_k - \mathbf{C}\hat{\mathbf{x}}_k^- && (2.12)
\end{aligned}$$

where $\hat{\mathbf{x}}_k^-$ and $\hat{\mathbf{P}}_k^-$ are the n-dimensional propagated state estimate vector and $n\,\mathrm{x}\,n$ error covariance matrix conditioned on observation prior to k, respectively, $\hat{\mathbf{x}}_k$ and $\hat{\mathbf{P}}_k$ are the estimated same quantities after using the observation $\mathbf{y}_k$ and $\mathbf{K}_k$ is the Kalman gain. $\hat{\mathbf{R}}$ and $\hat{\mathbf{Q}}$ denote the estimated quantities of the noise statistics in Eqs. (2.4) and (2.3), respectively.

2.2 Noise statistics effect

The effect of *a priori* unknown noise statistics on the estimation process is reviewed here. The noise statistics refer to:

- The process noise covariance, $\mathbf{Q}$.
- The measurement noise covariance, $\mathbf{R}$.

This evaluation was performed by first simulating a trajectory described by Eqs. (2.1) and (2.2). The measurements $\mathbf{y}_k$ obtained from this simulation, the initial *a priori* estimate $\hat{\mathbf{x}}_0$ and its associated state error covariance $\hat{\mathbf{P}}_0$ were the initial conditions for starting the estimation process.
As long as the noise statistics are assumed stationary (do not change over time), the Kalman gain converges to a steady-state gain denoted by $\mathbf{K}$ (the subscript k is omitted). Similarly, the error covariance matrices are also steady and the subscripts can be dropped.
The availability of the actual state vector $\mathbf{x}_k$ allowed to compute the actual error covariance matrix, i.e.:

$$\mathbf{P}_{\text{actual}} = \mathbb{E}\left\{(\mathbf{x}_k - \hat{\mathbf{x}}_\mathbf{k})(\mathbf{x}_k - \hat{\mathbf{x}}_\mathbf{k})^T\right\} \tag{2.13}$$

Moreover, the Kalman filter provides an estimate of this quantity (see Eq. (2.11)). Then, an element-wise comparison between these two matrices is interesting, in particular between the (1,1) elements, as they are the error variance of the first state vector component. Therefore, the effect of a wrong noise statistic in the initialization of the Kalman filter can be observed with these quantities. In addition, two quotients between the (1,1) elements of the error covariance matrices are interesting. The first refers to the reliability of $[\hat{\mathbf{P}}]_{1,1}$, i.e.:

$$\frac{[\hat{\mathbf{P}}]_{1,1}}{[\mathbf{P}_{\text{actual}}]_{1,1}} \tag{2.14}$$

This quantity indicates in how much the estimated error variance by the Kalman filter differs from the actual. Of course, if this quotient is larger than 1, that would indicate that the estimated error variance is larger than the actual.
Similarly, another interesting quotient is that comparing the actual error variance to the optimum error variance, i.e., the error variance resulting from estimating using the actual noise covariances:

$$\frac{[\mathbf{P}_{\text{actual}}]_{1,1}}{[\mathbf{P}_{\text{optimum}}]_{1,1}} \tag{2.15}$$

This last quotient is a measure of the performance loss because of using wrong noise covariances in the estimation.

2.2.1 Trajectory simulation

Prior to the estimation process, it was necessary to generate a trajectory with known noise statistics and state vector. That was achieved by implementing Eqs. (2.1) and (2.2) in MATLAB for a $n = 2$-dimensional state vector and a $p = 1$-dimensional measurement vector. The length of the trajectory was chosen to be 10^4 samples. The integral time T_i is 1 ms to make it similar to the minimum predetection integration interval in a GPS receiver tracking loop for the L1 carrier.
For that particular case of a $p = 1$-dimensional measurement vector, the measurement noise statistical properties are given by:

$$\mathbb{E}\left\{\mathbf{v}_i\right\} = 0, \quad \mathbb{E}\left\{\mathbf{v}_i {\mathbf{v}_j}^T\right\} = r\mathbf{I}_p\delta_{ij}, \tag{2.16}$$

where r is the measurement noise variance and $\mathbf{I}_p$ denotes the p-dimensional identity matrix.
For the process noise vector $\mathbf{w}_k$, it must be satisfied that:

$$\mathbf{w}_k \sim \mathcal{N}(\mathbf{0}, \mathbf{Q}), \tag{2.17}$$

where $\mathbf{Q}$ is defined as the process noise covariance matrix. Then, a way of obtaining $\mathbf{w}_k$ is by:

$$\mathbf{w}_k = \mathbf{L}^T\mathbf{z}_k, \tag{2.18}$$

where $\mathbf{L}$ is a lower triangular matrix with strictly positive diagonal entries obtained by the Cholesky decomposition of $\mathbf{Q}$ (i.e., $\mathbf{Q} = \mathbf{L}^T\mathbf{L}$) and $\mathbf{z}_k \sim \mathcal{N}(0, \mathbf{I})$ for $k = 1, \ldots, 10^4$.

2.2.2 Different process noise evaluation

Once a trajectory was generated, the estimation process was performed for different process noise covariances. These different process noise covariances were in fact scaled versions of the actual process noise $\mathbf{Q}$ used in the generation of the trajectory. Therefore, a process noise scale factor q was defined as:

$$\hat{\mathbf{Q}} = q\mathbf{Q}, \tag{2.19}$$

where $\hat{\mathbf{Q}}$ denotes the *a priori* estimated process noise covariance matrix. As explained above, the effect of this scaling factor q can be observed by comparing

the estimated error variance to the actual. Figure 2.1 illustrates the Kalman filter's $\hat{\mathbf{P}}$ reliability for different scale factors. As expected, the estimated error variance $[\hat{\mathbf{P}}]_{1,1}$ is equal to the actual when estimating using the correct process noise variance. Furthermore, it is more desirable to perform the estimation for $q > 1$ as the estimated error variance does not degrade that much from the actual error variance. Similarly, Figure 2.2 shows the performance loss when using a

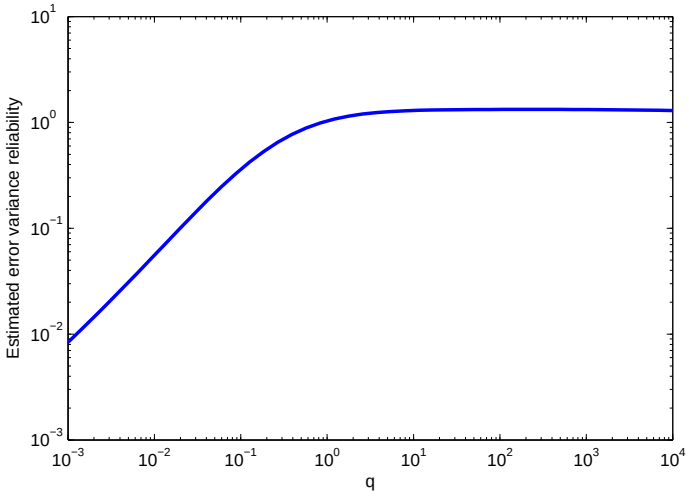

Figure 2.1: Estimated error variance reliability ($[\hat{\mathbf{P}}]_{1,1}/[\mathbf{P}_{\text{actual}}]_{1,1}$) when using a wrong process noise covariance averaged for 20 trajectories; 50 scale factors evaluated

wrong process noise. Of course, the optimum performance is for the actual process noise, but a different scaled version of it would result in a significant degradation of the performance.

2.2.3 Different measurement noise evaluation

It would be also interesting to plot the same quantities as in Figs. 2.1 and 2.2 for different scaled versions of the actual process noise variance r (i.e., $\hat{r} = \rho r$) and a fixed process noise covariance equal to the actual one (i.e., $\hat{\mathbf{Q}} = \mathbf{Q}$). Figures 2.3 and 2.4 are the resulting plots. The reliability of the estimated error variance is more affected compared to before, while the performance loss still appears whenever the measurement noise is different from the actual. The reason that Figs. 2.2 and 2.4 look identically but mirrored is because a non-trivial property of the Kalman gain. An alternative expression for Eq. (2.11) is [3]:

$$\hat{\mathbf{P}}_k = \mathbf{A}\left(\hat{\mathbf{P}}_k - \hat{\mathbf{P}}_k\mathbf{C}^T\left(\mathbf{C}\hat{\mathbf{P}}_k\mathbf{C}^T + \hat{\mathbf{R}}\right)^{-1}\mathbf{C}\hat{\mathbf{P}}_k\right)\mathbf{A}^T + \hat{\mathbf{Q}} \tag{2.20}$$

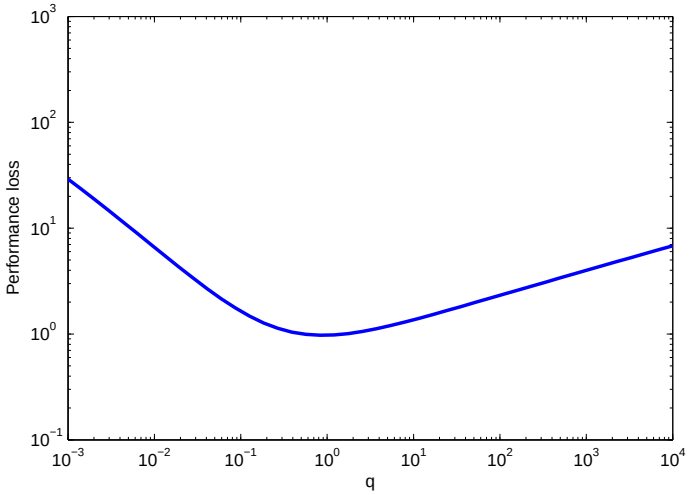

Figure 2.2: Performance loss ($[\mathbf{P}_{\text{actual}}]_{1,1}/[\mathbf{P}_{\text{optimum}}]_{1,1}$) for a Kalman filter when using a wrong process noise covariance averaged for 20 trajectories; 50 scale factors evaluated

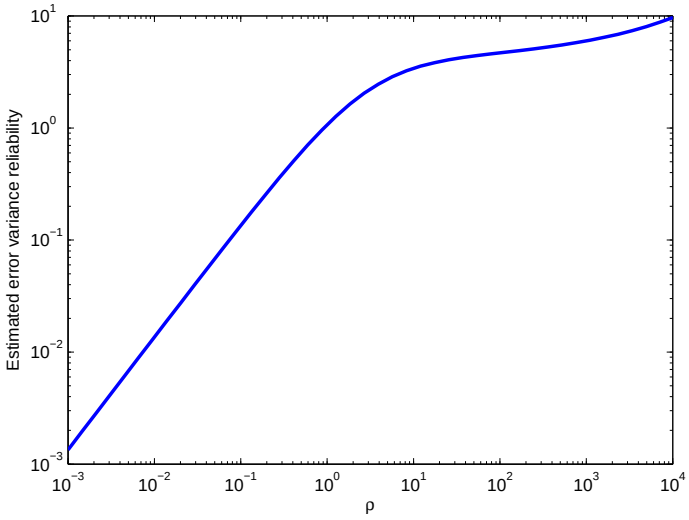

Figure 2.3: Estimated error variance reliability ($[\hat{\mathbf{P}}]_{1,1}/[\mathbf{P}_{\text{actual}}]_{1,1}$) when using a wrong measurement noise covariance averaged for 20 trajectories; 50 scale factors evaluated

For a scaled version of the noise covariance matrices (i.e., $\hat{\mathbf{R}}' = \alpha\hat{\mathbf{R}}$ and $\hat{\mathbf{Q}}' = \alpha\hat{\mathbf{Q}}$):

$$\begin{aligned}\hat{\mathbf{P}}_{k|\alpha} &= \mathbf{A}\left(\hat{\mathbf{P}}_{k|\alpha} - \hat{\mathbf{P}}_{k|\alpha}\mathbf{C}^T\left(\mathbf{C}\hat{\mathbf{P}}_{k|\alpha}\mathbf{C}^T + \alpha\hat{\mathbf{R}}\right)^{-1}\mathbf{C}\hat{\mathbf{P}}_{k|\alpha}\right)\mathbf{A}^T + \alpha\hat{\mathbf{Q}} \\ &= \alpha\hat{\mathbf{P}}_k \end{aligned} \tag{2.21}$$

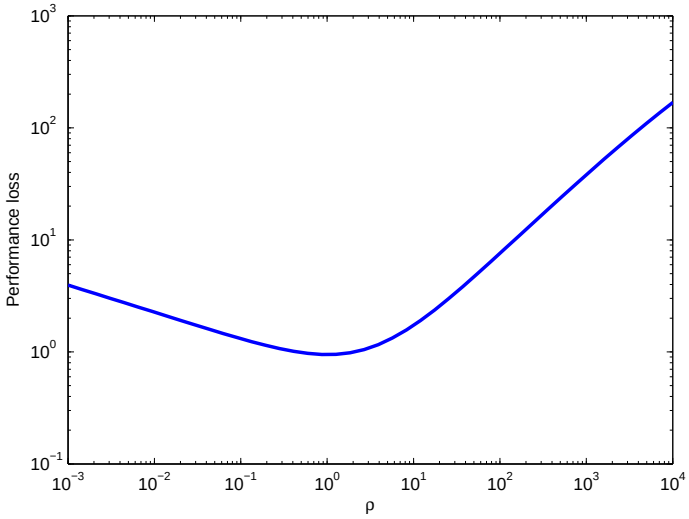

Figure 2.4: Performance loss ($[\mathbf{P}_{\text{actual}}]_{1,1}/[\mathbf{P}_{\text{optimum}}]_{1,1}$) for a Kalman filter when using a wrong measurement noise covariance averaged for 20 trajectories; 50 scale factors evaluated

Similarly, Eq. (2.8) for a scaled version of the noise matrices is:

$$\hat{\mathbf{P}}_{k|\alpha}^{-} = \alpha\hat{\mathbf{P}}_{k}^{-} \tag{2.22}$$

Substituting (2.22) in (2.9):

$$\mathbf{K}_{\alpha} = \hat{\mathbf{P}}_{k|\alpha}^{-}\mathbf{C}^{T}\left[\mathbf{C}\hat{\mathbf{P}}_{k|\alpha}^{-}\mathbf{C}^{T} + \alpha\hat{\mathbf{R}}\right]^{-1} = \mathbf{K} \tag{2.23}$$

Therefore, the scaling of $\mathbf{R}$ and $\mathbf{Q}$ by α results in a scaled error covariance matrix $\mathbf{P}$ scaled by α, but the scaling has no impact on the Kalman gain. □

2.3 State-vector dimension mismatch effect

Another particular evaluation is that regarding a different dimension between the state estimate vector and the actual process state vector, i.e., $n_{\text{traj}} \neq n_{\text{estim}}$. For a higher dimension in the state estimate vector than in the process state vector ($\dim(\mathbf{x}) < \dim(\hat{\mathbf{x}})$), it is interesting to quantify the effect of the *exceeding* component(s) on the first state vector component. Similarly to Section 2.2.2, Figure 2.5 shows the performance loss for a $n_{\text{traj}} = 2$-dimensional trajectory state vector and $n_{\text{estim}} = 3$-dimensional state estimate vector and different process noise covariances. For $\dim(\mathbf{x}) > \dim(\hat{\mathbf{x}})$, Figure 2.6 shows the same quotient for a $n_{\text{traj}} = 2$-dimensional trajectory state vector and $n_{\text{estim}} = 1$-dimensional state estimate vector.

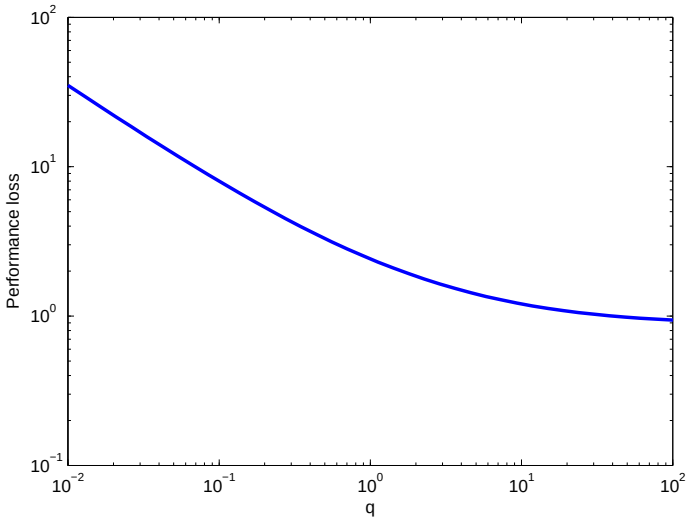

Figure 2.5: Performance loss for a $n_{\text{traj}} = 2$-dimensional trajectory state vector and $n_{\text{estim}} = 3$-dimensional state estimate vector and different process noise covariances (averaged for 20 trajectories; 50 scale factors evaluated)

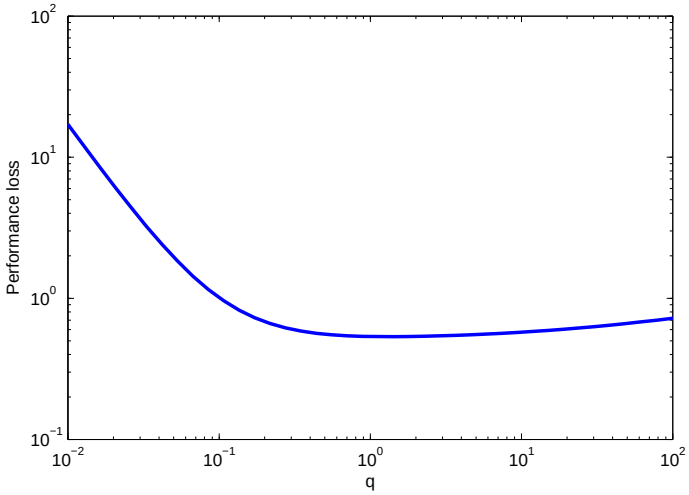

Figure 2.6: Performance loss for a $n_{\text{traj}} = 2 = 2$-dimensional trajectory state vector and $n_{\text{estim}} = 1$-dimensional state estimate vector and different process noise covariances (averaged for 20 trajectories; 50 scale factors evaluated)

Chapter 3

Adaptive Kalman Filtering

Chapter 2 has demonstrated that a Kalman filter requires an exact knowledge of the process noise covariance matrix $\mathbf{Q}$ and the measurement noise covariance matrix $\mathbf{R}$. Moreover, the use of wrong *a priori* statistics in the design of a Kalman filter can lead to large estimation errors. Therefore, these statistics should be checked at regular intervals and *adapted* accordingly. Otherwise the Kalman filter would be said to perform *suboptimally*. Different approaches in adaptive filtering are discussed in [1]. These adaptive methods are divided into:

- Bayesian estimation. For a vector $\boldsymbol{\alpha}$ of unknown parameters in the system, recursive equations for the *a posteriori* probability density of $\mathbf{x}_k$ and $\boldsymbol{\alpha}$ are obtained for $p(\mathbf{x}_k, \boldsymbol{\alpha}|\mathbf{Y}^k) = p(\mathbf{x}_k|\boldsymbol{\alpha}, \mathbf{Y}^k)p(\boldsymbol{\alpha}|\mathbf{Y}^k)$, where $p(\mathbf{x}_k|\boldsymbol{\alpha}, \mathbf{Y}^k)$ is Gaussian with mean $\hat{\mathbf{x}}_k$ and covariance $\hat{\mathbf{P}}_k(\boldsymbol{\alpha})$ obtained from the Kalman filter, and $\mathbf{Y}^k = \{\mathbf{y}_1, \ldots, \mathbf{y}_k\}$ is the measurement set until the time instant k.
- Maximum likelihood (ML) estimation. The ML likelihood of $\boldsymbol{\alpha}$ can be obtained by maximizing the marginal density $p(\boldsymbol{\alpha}|\mathbf{Y}^k)$ with respect to $\boldsymbol{\alpha}$.
- Correlation methods. These methods are mainly applicable to constant coefficient systems and consider the autocorrelation function of the output $\mathbf{y}_k$ or the autocorrelation function of the innovation sequence $\boldsymbol{\nu}_k$. The estimates from considering the innovation sequence are more efficient than those obtained from the output $\mathbf{y}_k$ since the innovation sequence is less correlated.
- Covariance-matching techniques. These techniques make the innovation sequence consistent with its theoretical covariance and modify the noise statistics accordingly to bring the actual covariance to the theoretical.

Only the innovation correlation methods are considered here.

3.1 Innovation correlation methods

In Kalman filtering, the innovation sequence (also known as *observational residual* or *residual sequence*) is defined as:

$$\boldsymbol{\nu}_k = \mathbf{y}_k - \mathbf{C}\hat{\mathbf{x}}_k^- \tag{3.1}$$

This quantity appears in Eq. (2.10) and it is said to bring the new information (i.e., the innovation) from the measurement $\mathbf{y}_k$ into the state estimate of $\hat{\mathbf{x}}_k$.

The interest in this quantity is that, for an *optimum* filter, this sequence appears to be zero-mean Gaussian white noise.

Proof. (After [4]). Let $\mathbf{e}_k^- = \mathbf{x}_k - \hat{\mathbf{x}}_k^-$ denote the error in estimating the *a priori* state. Then,

$$\boldsymbol{\nu}_k = \mathbf{C}\mathbf{e}_k^- + \mathbf{v}_k \tag{3.2}$$

The innovation autocorrelation function is defined as:

$$\begin{aligned}\boldsymbol{\Gamma}_l \equiv \mathbb{E}\left\{\boldsymbol{\nu}_k \boldsymbol{\nu}_{k-l}^T\right\} &= \mathbb{E}\left\{(\mathbf{C}\mathbf{e}_k^- + \mathbf{v}_k)(\mathbf{C}\mathbf{e}_{k-l}^- + \mathbf{v}_{k-l})^T\right\} \\ &= \mathbf{C}\mathbb{E}\left\{\mathbf{e}_k^- \mathbf{e}_{k-l}^-\right\}\mathbf{C}^T + \mathbf{C}\mathbb{E}\left\{\mathbf{e}_k^- \mathbf{v}_{k-l}^T\right\}, \quad \text{for } l > 0\end{aligned} \tag{3.3}$$

Using (2.1), (2.2), (2.7) and (2.10),

$$\begin{aligned}\mathbf{e}_k^- &= \mathbf{x}_k - \hat{\mathbf{x}}_k^- = \mathbf{A}\mathbf{x}_{k-1} + \mathbf{w}_{k-1} - \mathbf{A}\hat{\mathbf{x}}_{k-1} \\ &= \mathbf{A}\mathbf{x}_{k-1} + \mathbf{w}_{k-1} - \mathbf{A}\left(\hat{\mathbf{x}}_{k-1}^- + \mathbf{K}\left(\mathbf{y}_{k-1} - \mathbf{C}\hat{\mathbf{x}}_{k-1}^-\right)\right) \\ &= \mathbf{A}(\mathbf{I} - \mathbf{K}\mathbf{C})\mathbf{e}_{k-1}^- - \mathbf{A}\mathbf{K}\mathbf{v}_{k-1} + \mathbf{w}_{k-1}\end{aligned} \tag{3.4}$$

Iterating as in (3.4) l times,

$$\begin{aligned}\mathbf{e}_k^- = &\left[\mathbf{A}(\mathbf{I} - \mathbf{K}\mathbf{C})\right]^l \mathbf{e}_{k-l}^- - \sum_{j=1}^{l} \left[\mathbf{A}(\mathbf{I} - \mathbf{K}\mathbf{C})\right]^{j-1} \mathbf{A}\mathbf{K}\mathbf{v}_{k-j} \\ &+ \sum_{j=1}^{l} \left[\mathbf{A}(\mathbf{I} - \mathbf{K}\mathbf{C})\right]^{j-1} \mathbf{w}_{k-j}\end{aligned} \tag{3.5}$$

Postmultiplying (3.5) by ${\mathbf{e}_{k-l}^-}^T$ and calculating the expected value:

$$\mathbb{E}\left\{\mathbf{e}_k^- {\mathbf{e}_{k-l}^-}^T\right\} = \left[\mathbf{A}(\mathbf{I} - \mathbf{K}\mathbf{C})\right]^l \mathbf{P}^- \tag{3.6}$$

where $\mathbf{P}^-$ is the steady-state *a priori* error covariance matrix defined as:

$$\mathbf{P}^- = \mathbf{A}(\mathbf{I} - \mathbf{K}\mathbf{C})\mathbf{P}^-(\mathbf{I} - \mathbf{K}\mathbf{C})^T\mathbf{A}^T + \mathbf{A}\mathbf{K}\mathbf{R}\mathbf{K}^T\mathbf{A}^T + \mathbf{Q} \tag{3.7}$$

The previous equation is the algebraic Riccati equation for an optimum filter. The recursive equations in a Kalman filter converge the error covariance matrix $\hat{\mathbf{P}}_k^-$ satisfying this Riccati equation. Postmultiplying now (3.5) by $\mathbf{v}_{k-j}^T$ and calculating the expected value:

$$\mathbb{E}\left\{\mathbf{e}_k^- \mathbf{v}_{k-l}^T\right\} = -\left[\mathbf{A}(\mathbf{I} - \mathbf{K}\mathbf{C})\right]^{l-1} \mathbf{A}\mathbf{K}\mathbf{R} \tag{3.8}$$

Notice that the term:

$$\textstyle\sum_{j=1}^{l} \left[\mathbf{A}(\mathbf{I} - \mathbf{K}\mathbf{C})\right]^{j-1} \mathbf{A}\mathbf{K}\mathbf{v}_{k-j}$$

in Eq. (3.5), when postmultiplied by $\mathbf{v}_{k-l}^T$, makes a contribution only when $j = l$.
Inserting Eqs. (3.6) and (3.8) into (3.3):

$$\boldsymbol{\Gamma}_l = \mathbf{C}\left[\mathbf{A}(\mathbf{I} - \mathbf{K}\mathbf{C})\right]^{l-1} \mathbf{A}\left[\mathbf{P}^-\mathbf{C}^T - \mathbf{K}(\mathbf{C}\mathbf{P}^-\mathbf{C}^T + \mathbf{R})\right], \quad l > 0 \tag{3.9}$$

When $l = 0$,

$$\boldsymbol{\Gamma}_0 = \mathbf{C}\mathbf{P}^-\mathbf{C}^T + \mathbf{R} \tag{3.10}$$

From (3.9) and (3.10), it is seen that the autocorrelation function of $\boldsymbol{\nu}_k$ does not depend on k. Therefore, $\boldsymbol{\nu}_k$ is a *stationary* random sequence.
For an optimum gain $\mathbf{K}_{\text{op}}$, i.e., $\mathbf{K}_{\text{op}} = \mathbf{P}^{-}\mathbf{C}^T\left[\mathbf{C}\mathbf{P}^{-}\mathbf{C}^T + \mathbf{R}\right]^{-1}$, Eq. (3.9) equals 0 for all $l \neq 0$. Then, for this assumption of optimum gain, $\boldsymbol{\nu}_k$ is *white noise*.
Finally, since $\boldsymbol{\nu}_k$ is a linear sum of Gaussian random variables (i.e., $\mathbf{v}_k$), it is also *Gaussian*. □

As an example, Figure 3.1 illustrates the normalized autocorrelation function and power spectral density function of an innovation sequence $\boldsymbol{\nu}_k$ for an optimum Kalman filter. Clearly, the autocorrelation peak appears for a time lag $l = 0$, while the correlation vanishes rapidly for all $l \neq 0$.

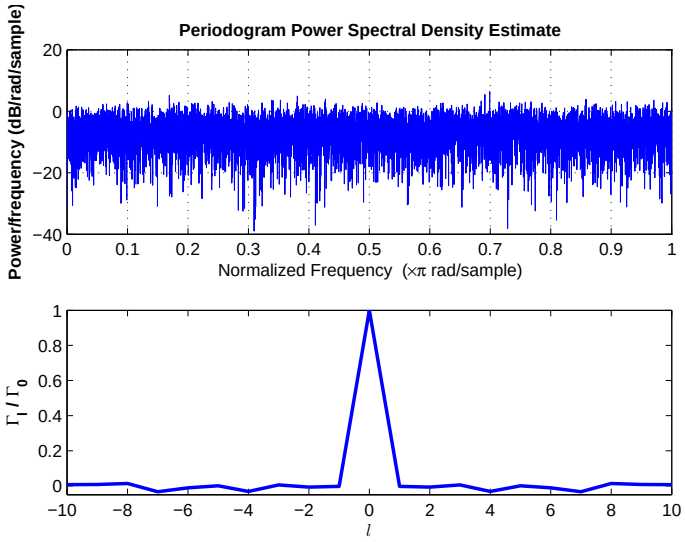

Figure 3.1: Normalized autocorrelation function and power spectral density of an innovation sequence for an optimum Kalman filter

3.1.1 Whiteness test for the innovation sequence

In Section 3.1, it has been demonstrated that the innovation sequence $\boldsymbol{\nu}_k$ is a zero-mean stationary white noise Gaussian sequence for an optimum filter. However, for a suboptimum filter, the innovation sequence is correlated as in Eqs. (3.9) and (3.10).
For an innovation-based adaptive algorithm, it would be necessary to check the statistics of this innovation sequence in order to determine the performance of the Kalman filter. A reliable measure is to check whether or not the sequence is white. Therefore, a test of *whiteness* should be performed upon the innovation sequence. The statistical hypothesis test from [6] is an example. Hypothesis testing is a process of establishing the validity of a hypothesis and to decide whether or not a hypothesis holds for a certain set of parameters of a statistical model.

For the particular case of a one-dimensional innovation sequence $\boldsymbol{\nu}_k = \{\nu_1, \ldots, \nu_N\}^T$, the Ljung-Box test states that the test statistic [6]:

$$Q_{\mathrm{LB}} = N(N+2)\sum_{l=1}^{m}(N-l)^{-1}\left(\frac{\hat{\Gamma}_l}{\hat{\Gamma}_0}\right)^2 \tag{3.11}$$

where

$$\hat{\Gamma}_l = \frac{1}{N}\sum_{j=l}^{N}\nu_j\nu_{j-l}^T \tag{3.12}$$

would for a large sample size N be distributed as χ^2_m since the estimates of the autocorrelation function $\left\{\hat{\Gamma}_1/\hat{\Gamma}_0, \ldots, \hat{\Gamma}_m/\hat{\Gamma}_0\right\}$ are multivariate normal with zero mean, $\mathrm{Var}(\hat{\Gamma}_l/\hat{\Gamma}_0) = (N-l)/(N(N+2))$ and $\mathrm{Cov}(\hat{\Gamma}_i, \hat{\Gamma}_j) = 0$ for $i \neq j$. The hypothesis that the innovation samples $\nu_1, \ldots, \nu_N$ are independent and identically distributed (i.i.d.) is *rejected* at a significance level α if $Q_{\mathrm{LB}} > \chi^2_{1-\alpha,m}$, where $\chi^2_{1-\alpha,m}$ is the $1-\alpha$ quantile of the chi-squared distribution with m degrees of freedom.
For the purpose of determining the whiteness of the innovation samples $\nu_1, \ldots, \nu_N$, it was enough to consider a number of lags m significantly smaller than the sample size ($m \ll N$), but larger than 1. The value of this number of lags used in the implementation is $m = 15$ for a sample size of $N = 1000$.

3.2 Estimation of Q and R

For the estimation of $\mathbf{Q}$ and $\mathbf{R}$, different algorithms were implemented for a Kalman filter of the form (2.7-2.11) for a $n = 2$-dimensional state vector and $p =$ 1-dimensional measurement vector. For both the simulation of the trajectory and the Kalman filter estimation, the noise statistical properties are:

$$\mathbb{E}\{\mathbf{v}_i\} = 0, \quad \mathbb{E}\left\{\mathbf{v}_i{\mathbf{v}_j}^T\right\} = r\mathbf{I}_p\delta_{ij} \tag{3.13}$$

$$\mathbb{E}\{\mathbf{w}_i\} = 0, \quad \mathbb{E}\left\{\mathbf{w}_i{\mathbf{w}_j}^T\right\} = \mathbf{Q}\delta_{ij} \tag{3.14}$$

$$\mathbb{E}\left\{\mathbf{v}_i{\mathbf{w}_j}^T\right\} = \mathbf{0}_{p\mathrm{x}n}, \quad \text{for any } i \text{ and } j \tag{3.15}$$

where r is defined as the measurement noise *variance* in units of rad^2, $\mathbf{Q}$ is the process noise covariance matrix and $\mathbf{I}_p$ denotes the p-dimensional identity matrix. From Eq. (3.15), it is assumed an uncorrelated noise model. Finally, the integral time T_i is 1 ms (minimum predetection integral time in a GPS receiver phase tracking loop for the L1 carrier).
For a N sample size of the innovation sequence, an estimate of the autocorrelation function is obtained as in Eq. (3.12). The estimates $\hat{\Gamma}_l$ are biased for a finite sample size according to:

$$\mathbb{E}\left\{\hat{\Gamma}_l\right\} = (1 - l/N)\Gamma_l \tag{3.16}$$

However, this estimate is preferable since the mean-square error is smaller than for the unbiased estimate ([5]).

3.2.1 Estimation of r from Mehra ([4])

For the algorithm in [4], an estimate of the measurement noise variance, r, is obtained from Eq. (3.10):

$$\hat{r} = \hat{\Gamma}_0 - \mathbf{C}(\mathbf{P}^{-}\mathbf{C}^T) \tag{3.17}$$

The problem of obtaining an estimate of r from Eq. (3.17) is that there is no availability of the *actual* steady-state error covariance matrix $\mathbf{P}^{-}$, but to the Kalman filter estimate of it, $\hat{\mathbf{P}}^{-}$. However, an estimate of r can be obtained by inserting (3.10) in (3.9) for $l = 1$ and $l = 2$, leading to:

$$\mathbf{P}^{-}\mathbf{C}^T = \mathbf{K}\Gamma_0 + \mathbf{D}^{+}\begin{bmatrix}\Gamma_1 \\ \Gamma_2\end{bmatrix} \tag{3.18}$$

where

$$\mathbf{D} = \begin{bmatrix}\mathbf{CA} \\ \mathbf{CA}(\mathbf{I} - \mathbf{KC})\mathbf{A}\end{bmatrix} \tag{3.19}$$

and $(\,\cdot\,)^{+}$ denotes the pseudo-inverse matrix. Using the estimates of the auto-correlation function $\hat{\Gamma}_0$, $\hat{\Gamma}_1$ and $\hat{\Gamma}_2$ in Eq. (3.18), the matrix product $\mathbf{P}^{-}\mathbf{C}^T$ is estimated and it can be substituted back in Eq. (3.17). Figure 3.2 shows the estimates of r from the algorithm in [4].

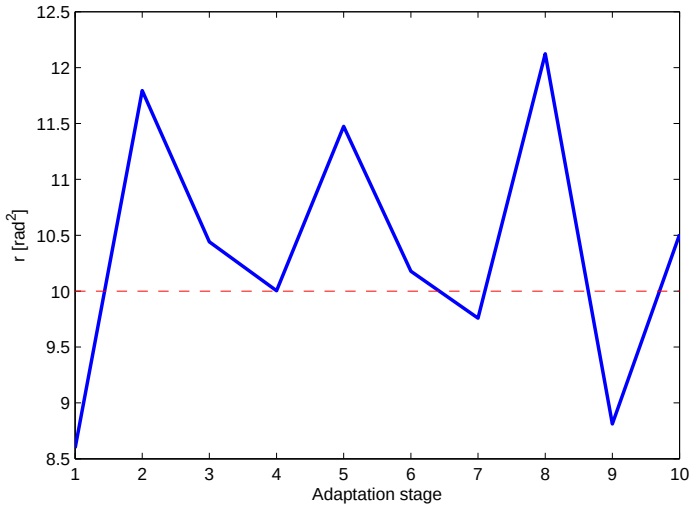

Figure 3.2: $\hat{r}$ estimates from the algorithm in [4]. Each adaptation stage is performed after 1000 samples. The actual value is $r = 10$ rad^2.

3.2.2 Estimation of r from Myers et al. ([7])

Similarly, the algorithm described in [7] computes an empirical estimator for the noise statistics from a sample realization of the measurements $\mathbf{y}_k$. At a given

observation time k, the measurement vector $\mathbf{y}_k$ is given by $\mathbf{y}_k = \mathbf{C}\mathbf{x}_k + \mathbf{v}_k$, where $\mathbf{v}_k \sim \mathcal{N}(0, \mathbf{R})$. Then, an intuitive approximation for $\mathbf{v}_k$ is given by:

$$\hat{\mathbf{v}}_k = \mathbf{y}_k - \mathbf{C}\hat{\mathbf{x}}_k^- \tag{3.20}$$

An unbiased estimator for r is obtained by first computing the sample mean and then an estimate of the covariance according to:

$$\bar{\mathbf{v}} = \frac{1}{N}\sum_{j=1}^{N}\hat{\mathbf{v}}_j \tag{3.21}$$

and

$$\mathrm{Cov}(\hat{\mathbf{v}}_k) = \frac{1}{N-1}\sum_{j=1}^{N}(\hat{\mathbf{v}}_j - \bar{\mathbf{v}})(\hat{\mathbf{v}}_j - \bar{\mathbf{v}})^T \tag{3.22}$$

Of course, the sample mean would tend to 0 for a large sample size N and the estimator of the covariance is biased with the expression:

$$\mathbb{E}\left\{\mathrm{Cov}(\hat{\mathbf{v}}_k)\right\} = \frac{1}{N}\sum_{j=1}^{N}\mathbf{C}\mathbf{P}_j^-\mathbf{C}^T + \mathbf{R} \tag{3.23}$$

Solving the previous equation for $\mathbf{R}$ and considering the estimated quantities of each term, an unbiased estimate of $\mathbf{R}$ is given by:

$$\hat{\mathbf{R}} = \frac{1}{N-1}\sum_{j=1}^{N}\left[(\hat{\mathbf{v}}_j - \bar{\mathbf{v}})(\hat{\mathbf{v}}_j - \bar{\mathbf{v}})^T - \left(\frac{N-1}{N}\right)\mathbf{C}\hat{\mathbf{P}}_j^-\mathbf{C}^T\right] \tag{3.24}$$

For the particular case of a one-dimensional measurement vector, Figure 3.3 shows the estimates of r using this algorithm.

3.2.3 Estimation of Q from Mehra ([4])

The adaptive algorithm in [4] presents also a method for obtaining an estimate of the process noise covariance matrix $\mathbf{Q}$.
According to [4], an estimate of $\mathbf{Q}$ can be obtained with the set of equations:

$$\begin{aligned}\sum_{j=0}^{i-1}\mathbf{C}\mathbf{A}^j\mathbf{Q}(\mathbf{A}^{j-i})^T\mathbf{C}^T = \mathbf{C}\mathbf{P}^-(\mathbf{A}^{-i})^T\mathbf{C}^T - \mathbf{C}\mathbf{A}^i\mathbf{P}^-\mathbf{C}^T \\ -\sum_{j=0}^{i-1}\mathbf{C}\mathbf{A}^j\hat{\mathbf{\Omega}}(\mathbf{A}^{j-i})^T\mathbf{C}^T, \qquad i = 1, \ldots, n\end{aligned} \tag{3.25}$$

where

$$\hat{\mathbf{\Omega}} = \mathbf{A}\left[-\mathbf{K}\mathbf{C}\mathbf{P}^- - \mathbf{P}^-\hat{\mathbf{C}}^T\mathbf{K}^T + \mathbf{K}\hat{\Gamma}_0\mathbf{K}^T\right]\mathbf{A}^T \tag{3.26}$$

The term $\mathbf{P}^-\mathbf{C}^T$ in (3.25) is the same as in (3.18) and it is treated and estimated as a single term. For that reason, Eq. (3.25) can be completely solved for $\mathbf{Q}$ because of the property $\left(\mathbf{P}^-\mathbf{C}^T\right)^T = \mathbf{C}\mathbf{P}^-$.
The expression (3.25) is obtained by substituting back for $\mathbf{P}^-$ (i.e., the *actual* steady-state error covariance matrix) in Eq. (3.7) 2 times and premultiplying

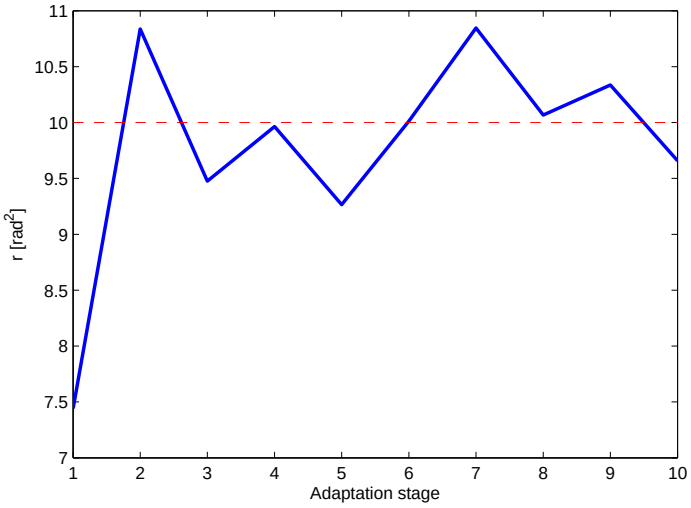

Figure 3.3: $\hat{r}$ estimates from the algorithm in [7]. Each adaptation stage is performed after 1000 samples. The actual value is $r = 10$ rad^2.

and postmultiplying both sides by $\mathbf{C}$ and $\mathbf{A}^{-k}\mathbf{C}^T$, respectively. By performing these multiplications, the right-hand side of (3.25) is completely determined from $\mathbf{P}^-\mathbf{C}^T$ and $\hat{\Gamma}_0$. However, the set of equations resulting is not linearly independent and a linear independent subset of these equations should be chosen. For the particular case of a $n = 2$-dimensional state vector,

$$\begin{aligned}\mathbf{C}\mathbf{Q}(\mathbf{A}^{-1})^T\mathbf{C}^T =& \hat{\mathbf{C}}\hat{\mathbf{M}}(\mathbf{A}^{-1})^T\mathbf{C}^T - \mathbf{C}\mathbf{A}\mathbf{P}^-\mathbf{C}^T \\ &- \mathbf{C}\hat{\mathbf{\Omega}}(\mathbf{A}^{-1})^T\mathbf{C}^T \end{aligned} \tag{3.27}$$

Substituting in Eq. (3.27) $\mathbf{Q}$ by $q_w\mathbf{Q}_0$ defined as (A.7):

$$\mathbf{Q}_0 = \begin{bmatrix} \frac{T_i^3}{3} & \frac{T_i^2}{2} \\ \frac{T_i^2}{2} & T_i \end{bmatrix} \tag{3.28}$$

and solving for the left-side part the product $\mathbf{C}\mathbf{Q}_0(\mathbf{A}^{-1})^T\mathbf{C}^T$ equals to:

$$\mathbf{C}\mathbf{Q}_0(\mathbf{A}^{-1})^T\mathbf{C}^T = \frac{q_w T_i^3}{12} \tag{3.29}$$

Despite the relative simplicity of Eq. (3.29), the results from several simulations showed that this algorithm fails to compute a consistent estimate of $\mathbf{Q}$. The reason would be probably in the effect of dealing with such a small integral time T_i (1 ms = 0.001 s). It should be recalled that the process noise covariance matrix is defined as:

$$\mathbf{Q} = q_w \begin{bmatrix} \frac{T_i^3}{3} & \frac{T_i^2}{2} \\ \frac{T_i^2}{2} & T_i \end{bmatrix} \tag{3.30}$$

Therefore, the components of this matrix take really small values compared to the noise variance q_w. Also, the state transition matrix $\mathbf{A}$ is defined as:

$$\mathbf{A} = \begin{bmatrix} 1 & T_i \\ 0 & 1 \end{bmatrix} \approx \begin{bmatrix} 1 & 0 \\ 0 & 1 \end{bmatrix} \tag{3.31}$$

By doing this approximation, the state transition matrix is a diagonal matrix. This would indicate that the i-th component in the state vector at time instant $k+1$ is only related with the i-th component in the state vector at time instant k, so there is not much contribution from the state noise vector (or at least its contribution is *obscured*).

3.2.4 Estimation of Q from Myers et al. ([7])

For the algorithm in [7], an intuitive approximation of the process noise statistics is obtained from a sample realization of $\hat{\mathbf{x}}$ by:

$$\hat{\mathbf{w}}_{k-1} = \hat{\mathbf{x}}_k - \mathbf{A}\hat{\mathbf{x}}_{k-1} \tag{3.32}$$

As previously, the *unbiased* estimator for $\mathbf{Q}$ is obtained by:

$$\hat{\mathbf{Q}} = \frac{1}{N-1}\sum_{j=1}^{N}\left[(\hat{\mathbf{w}}_j - \bar{\mathbf{w}})(\hat{\mathbf{w}}_j - \bar{\mathbf{w}})^T - \frac{N-1}{N}\left(\mathbf{A}\hat{\mathbf{P}}_{j-1}\mathbf{A}^T - \hat{\mathbf{P}}_j\right)\right] \tag{3.33}$$

where $\bar{\mathbf{w}}$ is the unbiased sample mean of $\hat{\mathbf{w}}_k$ and $\hat{\mathbf{P}}_k$ the estimated error covariance matrix from the Kalman filter.
Assuming that the process noise is stationary over N samples and unbiased ($\bar{\mathbf{w}} = 0$), another expression for $\hat{\mathbf{Q}}$ from (3.33) can be obtained [8]. Recalling (3.32):

$$\begin{aligned} \hat{\mathbf{w}}_{k-1} &= \hat{\mathbf{x}}_k - \mathbf{A}\hat{\mathbf{x}}_{k-1} \\ &= \hat{\mathbf{x}}_k - \hat{\mathbf{x}}_k^- = \mathbf{K}\boldsymbol{\nu}_k \end{aligned} \tag{3.34}$$

The biased estimator of $\mathbf{Q}$ in (3.33) becomes:

$$\hat{\mathbf{Q}} = \frac{1}{N}\sum_{j=1}^{N}\left[\hat{\mathbf{w}}_j\hat{\mathbf{w}}_j^T - \left(\mathbf{A}\hat{\mathbf{P}}_{j-1}\mathbf{A}^T - \hat{\mathbf{P}}_j\right)\right] \tag{3.35}$$

Substituting (3.34) into (3.35):

$$\hat{\mathbf{Q}} = \frac{1}{N}\sum_{j=1}^{N}\left[\left(\mathbf{K}\boldsymbol{\nu}_j\boldsymbol{\nu}_j^T\mathbf{K}^T\right) - \left(\mathbf{A}\hat{\mathbf{P}}_{j-1}\mathbf{A}^T - \hat{\mathbf{P}}_j\right)\right] \tag{3.36}$$

Both estimators did not perform well probably because of the same reasons as in Section 3.2.3.

3.2.5 Estimation of Q and r from Bélanger ([9])

The last algorithm considered for the estimation of $\mathbf{Q}$ and $\mathbf{R}$ is that in [9]. This method is also an innovation correlation method and it states that if the covariance matrices are linear in a set of parameters, then the correlation function

of the innovation sequence is also a linear function of this set of parameters. Therefore, $\mathbf{Q}$ and $\mathbf{R}$ are regarded as linear functions of the M components of a vector $\boldsymbol{\alpha} = [\alpha_1, \ \ldots, \ \alpha_M]$, i.e.:

$$\mathbf{R} = \sum_{i=1}^{M} \mathbf{R}_i \alpha_i; \qquad \mathbf{Q} = \sum_{i=1}^{M} \mathbf{Q}_i \alpha_i \tag{3.37}$$

with $\mathbf{R}_i$ and $\mathbf{Q}_i$ known constant matrices. The problem is to find an estimate of $\boldsymbol{\alpha}$. The particular derivation of the algorithm in [9] is left for Appendix B. The estimates of $\boldsymbol{\alpha}$ depend on the algorithm design parameters, namely the number of shifts, L, and the sample size, N. Figure 3.4 shows the components of $\boldsymbol{\alpha}$ for different number of shifts for an innovation sample realization of 1000 samples and averaged for 10 trajectories. Similarly, Figure 3.5 shows the vari-

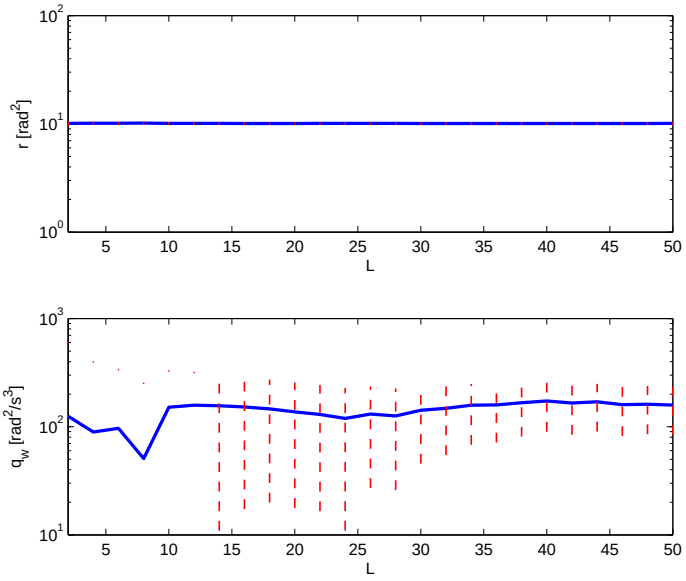

Figure 3.4: Components of $\boldsymbol{\alpha}$ from the algorithm in [9] for $L = 2, \ 4, \ \ldots, \ 50$. The actual values are $r = 10$ rad^2 and $q_w = 100$ rad^2/s^3. The sample size considered is $N = 750$. A standard deviation is plot in each side of the estimate.

ance estimates for different sample sizes. The dependency on this sample size is very intuitive: for a large sample size, the estimator of the innovation sequence autocorrelation function is less biased and the information contained in the innovation sequence is greater.

3.3 Direct estimation of the optimal gain

Section 3.1 has demonstrated that a filter is optimum when the innovation sequence is a zero-mean Gaussian white noise sequence. In addition, the Kalman

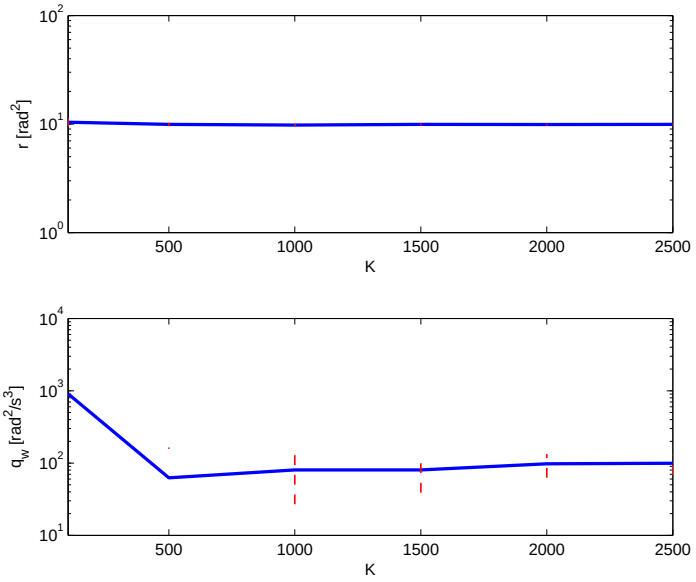

Figure 3.5: Components of $\boldsymbol{\alpha}$ from the algorithm in [9] for different K between 100 and 2500 in steps of 500. The actual values are $r = 10$ rad^2 and $q_w = 100$ rad^2/s^3. The number of time lags was set to $L = 25$. A standard deviation is plot in each side of the estimate.

gain for such a filter is also *optimal*.
The algorithms explained so far did not consider the *optimality* of the Kalman gain but the whiteness of the innovation sequence in order to obtain the estimates of the noise statistics. Therefore, the direct estimation of the optimal gain differs from the rest of adaptive filtering techniques. Moreover, it will be shown that the identification of this optimum gain does not involve $\mathbf{Q}$ or $\mathbf{R}$ and then the interest in these algorithms.
For the estimation of the optimal gain, the algorithms in [4] and [10] were considered.

3.3.1 Algorithm from Mehra ([4])

From [4], the estimation of the optimal gain $\mathbf{K}_{\text{op}}$ is based on the property that for a suboptimum gain $\mathbf{K}_0$, the error covariance matrix $\mathbf{P}_1^-$ associated to $\mathbf{K}_0$ satisfies:

$$\mathbf{P}_1^- = \mathbf{A}(\mathbf{I} - \mathbf{K}_0\mathbf{C})\mathbf{P}_1^-(\mathbf{I} - \mathbf{K}_0\mathbf{C})^T\mathbf{A}^T + \mathbf{A}\mathbf{K}_0\mathbf{R}\mathbf{K}_0^T\mathbf{A}^T + \mathbf{Q} \tag{3.38}$$

Similarly:

$$\mathbf{K}_1 = \mathbf{P}_1^-\mathbf{C}^T(\mathbf{C}\mathbf{P}_1^-\mathbf{C}^T + \mathbf{R})^{-1} \tag{3.39}$$

The error covariance matrix $\mathbf{P}_2^-$ associated to the gain $\mathbf{K}_1$ satisfies:

$$\mathbf{P}_2^- = \mathbf{A}(\mathbf{I} - \mathbf{K}_1\mathbf{C})\mathbf{P}_2^-(\mathbf{I} - \mathbf{K}_1\mathbf{C})^T\mathbf{A}^T - \mathbf{A}\mathbf{K}_1\mathbf{R}\mathbf{K}_1^T\mathbf{A}^T + \mathbf{Q} \tag{3.40}$$

Substracting (3.38) from (3.40):

$$\begin{aligned}(\mathbf{P}_2^- - \mathbf{P}_1^-) =& \mathbf{A}(\mathbf{I} - \mathbf{K}_1\mathbf{C})(\mathbf{P}_2^- - \mathbf{P}_1^-)(\mathbf{I} - \mathbf{K}_1\mathbf{C})^T\mathbf{A}^T \\ & -\mathbf{A}(\mathbf{K}_1 - \mathbf{K}_0)(\mathbf{C}\mathbf{P}_1^-\mathbf{C}^T + \mathbf{R})(\mathbf{K}_1 - \mathbf{K}_0)^T\mathbf{A}^T \end{aligned} \tag{3.41}$$

It can be shown that

$$\left[\mathbf{P}_2^-\right]_{ii} < \left[\mathbf{P}_1^-\right]_{ii} \tag{3.42}$$

Continuing with that gain and its associated error covariance matrix pair relationship:

$$\mathbf{K}_2 = \mathbf{P}_2^-\mathbf{C}^T(\mathbf{C}\mathbf{P}_2^-\mathbf{C}^T + \mathbf{R})^{-1} \tag{3.43}$$

and

$$\mathbf{P}_3^- = \mathbf{A}(\mathbf{I} - \mathbf{K}_2\mathbf{C})\mathbf{P}_3^-(\mathbf{I} - \mathbf{K}_1\mathbf{C})^T\mathbf{A}^T - \mathbf{A}\mathbf{K}_2\mathbf{R}\mathbf{K}_2^T\mathbf{A}^T + \mathbf{Q} \tag{3.44}$$

with $\left[\mathbf{P}_3^-\right]_{ii} < \left[\mathbf{P}_2^-\right]_{ii} < \left[\mathbf{P}_1^-\right]_{ii}$. These monotonically decreasing matrices must converge since it is bounded from below ($\mathbf{P}^- > 0$) and the sequence $\mathbf{K}_0, \mathbf{K}_1, \mathbf{K}_2, \ldots$ must converge to $\mathbf{K}_{\text{op}}$. For convergence of the Kalman filter, it is necessary that all the eigenvalues from $(\mathbf{I} - \mathbf{K}_1\mathbf{C})\mathbf{A}$ to be inside the unit circle[1].

Based on that, an iterative algorithm is constructed for estimating $\mathbf{K}_{\text{op}}$. Following the notation as in Sections 3.2.1 and 3.2.3, an estimate of $\mathbf{K}_1$ is obtained by:

$$\hat{\mathbf{K}}_\mathbf{1} = \mathbf{K}_0 + \mathbf{D}^+ \begin{bmatrix}\hat{\Gamma}_1 \\ \hat{\Gamma}_2\end{bmatrix} \hat{\Gamma}_0^{-1} \tag{3.45}$$

An estimate of $\delta\mathbf{P}_1^- \equiv \mathbf{P}_2^- - \mathbf{P}_1^-$ is obtained using:

$$\begin{aligned}\widehat{\delta\mathbf{P}_1^-} =& \mathbf{A}\left(\mathbf{I} - \hat{\mathbf{K}}_\mathbf{1}\mathbf{C}\right)\widehat{\delta\mathbf{P}_1^-}\left(\mathbf{I} - \hat{\mathbf{K}}_\mathbf{1}\mathbf{C}\right)^T\mathbf{A}^T \\ & -\mathbf{A}\left(\hat{\mathbf{K}}_\mathbf{1} - \mathbf{K}_0\right)\hat{\Gamma}_0\left(\hat{\mathbf{K}}_\mathbf{1} - \mathbf{K}_0\right)^T\mathbf{A}^T \end{aligned} \tag{3.46}$$

$\widehat{\delta\mathbf{P}_1^-}$ can be calculated recursively as in a Kalman filter. Moreover, an estimate of $\mathbf{K}_2$ and its associated error covariance matrix are obtained as follows:

$$\widehat{\mathbf{P}_\mathbf{2}^-\mathbf{C}^T} = \widehat{\mathbf{P}_\mathbf{1}^-\mathbf{C}^T} + \widehat{\delta\mathbf{P}_1^-}\mathbf{C}^T \tag{3.47}$$

$$\hat{\mathbf{K}}_2 = \widehat{\mathbf{P}_\mathbf{2}^-\mathbf{C}^T}\left(\mathbf{C}\widehat{\mathbf{P}_\mathbf{2}^-\mathbf{C}^T} + \hat{\mathbf{R}}\right)^{-1} \tag{3.48}$$

The implementation determined first if the innovation sequence was white or not prior to the adaptation. In [10] it is mentioned that the algorithm would not converge if the initial gain $\mathbf{K}_0$ is already the optimum gain. Moreover, as long as the innovation is almost white even for a wrong noise statistics, the adaptation was either not performed or converged to some destabilizing gain.

[1]The transfer function in the z-domain of a Kalman filter of the form in Eqs. (2.7 - 2.12) is:

$$H(\mathrm{z}) = \left[\mathrm{z}\mathbf{I} - (\mathbf{I} - \mathbf{K}\mathbf{C})\mathbf{A}\right]^{-1}\mathrm{z}\mathbf{K}$$

Therefore, the stability condition is all the eigenvalues from $(\mathbf{I} - \mathbf{K}\mathbf{C})\mathbf{A}$ to be inside the unit circle.

3.3.2 Algorithm from Carew et al. ([10])

The scheme in [10] is also an iterative algorithm to determine the optimum filter steady-state gain, $\mathbf{K}_{\text{op}}$, and the innovation sequence covariance matrix, $\mathbf{W}$, according to:

$$\begin{aligned}
\mathbf{W}(\mathbf{X}_m) &= \hat{\Gamma}_0 - \mathbf{C}\mathbf{X}_m\mathbf{C}^T && (3.49)\\
\mathbf{K}_m(\mathbf{X}_m) &= (\mathbf{\Theta}^+\mathbf{Z} - \mathbf{A}\mathbf{X}_m\mathbf{C}^T)\mathbf{W}^{-1}(\mathbf{X}_m) && (3.50)\\
\mathbf{X}_{m+1} &= (\mathbf{A}-\mathbf{K}\mathbf{C})\mathbf{X}_m(\mathbf{A}-\mathbf{K}\mathbf{C})^T \\
&\quad +(\mathbf{K}-\mathbf{K}_m(\mathbf{X}_m))\mathbf{W}(\mathbf{X}_m)(\mathbf{K}-\mathbf{K}_m(\mathbf{X}_m))^T && (3.51)
\end{aligned}$$

where:

$$\mathbf{\Theta}^T = \left[\mathbf{C}^T,\ \mathbf{A}^T\mathbf{C}^T\right] \tag{3.52}$$

is the system observability matrix and:

$$\mathbf{Z} = \begin{bmatrix} \hat{\Gamma}_1 + \mathbf{C}\mathbf{K}\hat{\Gamma}_0 \\ \hat{\Gamma}_2 + \mathbf{C}\mathbf{K}\hat{\Gamma}_1 + \mathbf{C}\mathbf{A}\mathbf{K}\hat{\Gamma}_0 \end{bmatrix} \tag{3.53}$$

As in the algorithm of Mehra, the previous set of equations converge $\mathbf{K}_m$ to $\mathbf{K}_{\text{op}}$ and $\mathbf{X}_m$ to the minimum error covariance matrix associated.
A simple choice for $\mathbf{X}_0$ is the null matrix. This is justified by the fact that $\mathbf{X} = \mathbf{0}$ if $\mathbf{K}_0$ happens to be equal to $\mathbf{K}_{\text{op}}$. Similar to the algorithm in [4], the adaptation was either not performed or the resulting gain was destabilizing.

3.4 Conclusions

The estimation of the measurement noise variance r from [4] and [7] has been shown to perform well. The first method requires to compute two lags of the autocorrelation function to obtain $\hat{r}$, which simplifies considerably the problem. However, it is based on the estimated quantity of a matrix product, i.e., $\mathbf{P}^-\mathbf{C}^T$. By contrast, the estimation of r from Myers et al. ([7]) is based on the actual measurement sequence $\mathbf{y}_k$ and the estimated error covariance matrix $\hat{\mathbf{P}}^-$.
The direct estimation of the optimal gain (see Section 3.3) has been seen to be sensitive to the computation of the autocorrelation of the innovation sequence. Moreover, for a wrong noise statistics initialization, the innovation sequence is almost white and thus the gain is close to the optimum gain, so for that reason there is no need of adaptation of the gain.
Moreover, the estimation of $\mathbf{Q}$ from Eqs. (3.33) and (3.36) appeared not to work. The reason would be probably the same as explained in Section 3.2.3.
Finally, the algorithm in [9] for the estimation of $\mathbf{Q}$ and $\mathbf{R}$ has demonstrated a good performance. Nevertheless, the algorithm design parameters should be chosen accordingly and their computational effort involved has to be considered.

Chapter 4

Carrier-phase Tracking

After acquisition, the Doppler frequency and code phase of all visible satellites are roughly determined. The purpose of signal tracking is to achieve a finer synchronization in order to condition the incoming signal for later processing. One method of tracking consists in tuning the carrier-phase of a locally generated copy and to mix it with the incoming signal. The difference (or offset) between the actual carrier-phase and that of the local copy is obtained from the output of a discriminator. Then, the frequency of the local copy is *proportionally* adjusted to that measure of the discriminator. This tracking scheme falls into the category of *carrier-phase tracking*.

4.1 Linearized digital second-order phase lock loop

For carrier-phase tracking, the most common scheme used is a phase lock loop (PLL). Figure 4.1 shows the block diagram of a linearized digital PLL. The

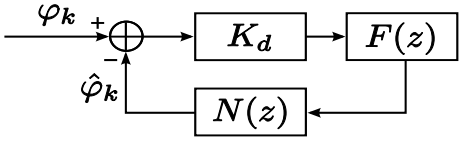

Figure 4.1: Linearized digital PLL model

transfer functions for the digital filter are:

$$F(\mathrm{z}) = \frac{(C_1 + C_2) - C_1 \mathrm{z}^{-1}}{1 - \mathrm{z}^{-1}} \tag{4.1}$$

$$N(\mathrm{z}) = \frac{K_0 \mathrm{z}^{-1}}{1 - \mathrm{z}^{-1}} \tag{4.2}$$

where $F(\mathrm{z})$ is the transfer function of a second-order PLL filter and $N(\mathrm{z})$ is the transfer function of the NCO. The gain of the NCO is K_0. The coefficients C_1

and C_2 from this filter are given by [11]:

$$C_1 = \frac{1}{K_0 K_d} \frac{8\zeta\omega_n T_i}{4(1+\zeta\omega_n T_i)+(\omega_n T_i)^2} \tag{4.3}$$

$$C_2 = \frac{1}{K_0 K_d} \frac{4(\omega_n T_i)^2}{4(1+\zeta\omega_n T_i)+(\omega_n T_i)^2} \tag{4.4}$$

where ζ is the damping ratio and ω_n is the natural frequency:

$$\omega_n = \frac{8\zeta B_L}{4\zeta^2+1} \tag{4.5}$$

where B_L is the noise bandwidth of the filter. Figure 4.2 shows in particular the form of a second-order PLL loop filter. The transfer function for the complete digital linearized filter is:

$$H(\mathrm{z}) = \frac{K_d F(\mathrm{z}) N(\mathrm{z})}{1 + K_d F(\mathrm{z}) N(\mathrm{z})} \tag{4.6}$$

where K_d is the gain of the phase discriminator. A PLL filter of the previous form contains different design parameters, namely the damping ratio ζ and the noise bandwidth B_L. The values of these quantities should be chosen accordingly by considering the effects of either large or small values. For example, a large value in the noise bandwidth B_L would result in a large noise component in the estimated phase, while a small value would slow the filter response and probably the filter will not settle down.

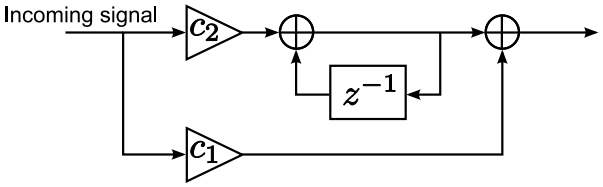

Figure 4.2: Second-order PLL

4.2 GNSS carrier-phase tracking loop filter

The implementation of a PLL filter of the form discussed in Section 4.1 in a GNSS receiver is by means of the scheme in Fig. 4.3. The purpose of a filter of that form is to combine the signals from the I and Q arms into a discriminator and obtain the phase error between the local carrier copy and the incoming signal. By performing this, the filter is insensitive to 180° phase shifts because of bit transitions and a direct measure of the phase error is obtained easily.
After the integral time $[t_{k-1},\ t_k]$, the in-phase and quadrature components at the output of the correlators can be approximated as [14]:

$$I_k \approx D_k R(\Delta\tau_k) \cdot \mathrm{sinc}\left(\frac{T_i}{2}\overline{\Delta\omega_n}\right) \cdot \cos\left(\overline{\Delta\phi_k}\right) + n_{I,k} \tag{4.7}$$

$$Q_k \approx D_k R(\Delta\tau_k) \cdot \mathrm{sinc}\left(\frac{T_i}{2}\overline{\Delta\omega_n}\right) \cdot \sin\left(\overline{\Delta\phi_k}\right) + n_{Q,k} \tag{4.8}$$

$$\tag{4.9}$$

where D_k refers to the navigation data sequence, $R(\Delta\tau_k)$ is the value of the autocorrelation function of the C/A code sequence offset by $\Delta\tau_k$, $\overline{\Delta\phi_k}$ and $\overline{\Delta\omega_n}$ are the average phase and frequency offsets, respectively, and $n_{I,k}$ and $n_{Q,k}$ are zero-mean uncorrelated Gaussian noise samples.
The discriminator combines the I_k and Q_k components to obtain the phase error between the local carrier copy and the incoming signal. There exist different forms of combining I_k and Q_k, but here it is assumed a discriminator of the form:

$$D = \tan^{-1}\left(\frac{Q_k}{I_k}\right) \tag{4.10}$$

From Equation (4.10), it can be seen that the phase error is minimized when the correlation in the quadrature-phase arm is zero and maximum in the in-phase. Moreover, the discriminator output can be approximated by:

$$D_O \approx \overline{\Delta\phi_k} + n_{D,k} \tag{4.11}$$

where $\overline{\Delta\phi_k}$ is the averaged phase error during the interval $[t_{k-1}, t_k]$ and $n_{D,k}$ is the measurement noise.
The steering of the local copy carrier-frequency f_k is achieved by the NCO from interval to interval in a continuous form, i.e.:

$$f_k = f_{k-1} + \delta f_{k,\mathrm{NCO}} \tag{4.12}$$

where $\delta f_{k,\mathrm{NCO}}$ represents the steering component of the frequency.

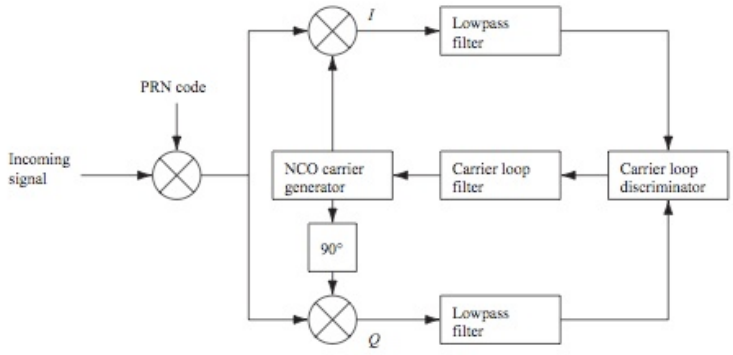

Figure 4.3: GNSS receiver carrier-phase loop tracking implementation

4.3 Kalman filter-based phase loop filter

The PLL filter presented in Section (4.1) is probably the most widely used form of a carrier-phase tracking architecture. Nevertheless, it could be seen that there exists a noise component in every signal component and stage of this filter. This noise component *corrupts* the deterministic part of the signal in order to model it closer to the actual signal dynamics.
A more powerful solution of phase tracking to that explained above is to model

the signal dynamics with a deterministic and non-deterministic component (the later corresponds to the noise component) and applying a linear least-squares filter accordingly. An example of a filter of that form is a Kalman filter (see Chapter 2).
This architecture turns the problem of phase tracking mainly into an estimation problem. Also, it is necessary to redefine the state propagation and estimation equations, the NCO model and the measurement model.

4.3.1 State propagation equation and controller form

The signal dynamics for a Kalman filter-based tracking architecture is described by Eq. (2.1). Nevertheless, the purpose of a tracking loop is to align the local copy to the incoming signal. That is achieved by some feedback mechanism that states the difference in either the carrier and code phase between copies. Thus the state vector is redefined in terms of residual errors as (see [12]):

$$\delta\mathbf{x}_k = \begin{bmatrix}\delta\phi_k \\ \delta f_k\end{bmatrix} = \begin{bmatrix}\phi_k - \phi_{\mathrm{NCO},k} \\ f_k - f_{\mathrm{NCO},k}\end{bmatrix} \tag{4.13}$$

The state propagation equation becomes:

$$\delta\mathbf{x}_{k+1} = \mathbf{A}\delta\mathbf{x}_k + \mathbf{B}_u\delta\mathbf{u}_k \tag{4.14}$$

where $\delta\mathbf{u}_k$ is the input update vector defined as:

$$\delta\mathbf{u}_k = \begin{bmatrix}\phi^+_{\mathrm{NCO},k} - \phi^-_{\mathrm{NCO},k} \\ f^+_{\mathrm{NCO},k} - f^-_{\mathrm{NCO},k}\end{bmatrix} \tag{4.15}$$

where $(\,\cdot\,)^-_{\mathrm{NCO},k}$ denotes the NCO parameter at time k and $(\,\cdot\,)^+_{\mathrm{NCO},k}$ denotes the updated NCO parameter after applying the control input. This control input contains the two states (phase and frequency) that the NCO steers upon the copy. Thus a controller prior to the NCO is necessary and of the form:

$$\mathbf{u}_k = -\mathbf{\Gamma}_{\mathrm{NCO}}\delta\hat{\mathbf{x}}_k \tag{4.16}$$

Similarly, the input propagation matrix $\mathbf{B}_u$ is:

$$\mathbf{B}_u = \begin{bmatrix}-1 & 0 \\ 0 & -1\end{bmatrix} \tag{4.17}$$

4.3.2 Measurement model

The measurement model can be described as in Eq. (2.2) but in terms of residual errors. Moreover, a direct measurement is that from the output of a discriminator of the form in Eq. (4.10), as it is directly the error in the phase and an additive noise term.

Chapter 5

Adaptive Kalman Filter-Based Phase Lock Loop GPS Receiver Implementation

Chapter 4 introduced the Kalman filter-based phase lock loop architecture. The scope of this chapter is to evaluate some of the adaptive algorithms presented in Chapter 3 for the case of phase tracking. From the results and conclusions in Chapter 3, only the following algorithms have been selected for the receiver implementation:

- Estimation of r from Mehra ([4]).
- Estimation of q_w and r from Bélanger ([9]).

5.1 Methodology

The algorithms implemented are innovation correlation methods of adaptive filtering. That implies to consider a finite sample size of the innovation sequence. Moreover, it will be demonstrated that the results depend on this sample size. For that reason, it was necessary to evaluate the algorithms for different innovation sample sizes. Of course, the larger the sample size, the more accurate is the innovation autocorrelation function determined, but the more computing effort necessary.
The algorithms were implemented in a software-defined GPS receiver in MATLAB. The code performed the acquisition and tracking from recorded data contained in a .sim format file. Both acquisition and tracking were performed serially, i.e., one channel (satellite) at a time. After tracking, the results were stored in a .mat file for later post-processing.
The recorded data corresponds to real GPS measurements from two different measurement campaigns. Table 5.1 summarizes the date, place and some other details from these measurement campaigns.

Measurement campaign	Measurement campaign corresponding to the work of Giger et al. [13]	**Place and date:**	En-route flight near Hof (DE) and Innsbruck (AT) - 15/12/2008
		Scenarios:	2 - gnd/acft
		Antenna:	Antcom 42GO1116A2-XT-1 (acft) / Javad MarAnt (gnd)
		Receiver/software:	NordNav R-30/NordNav-Rx
		Sampling freq.:	1.63676 [MHz] (L1 carrier)
		Coordinates:	long = 11.35, lat = 47.26, height = 637 m (gnd)
	Measurement campaign around the Technische Universität München (TUM), München	**Place and date:**	München (DE) - 28/06/2010
		Scenarios:	5 - scenX
		Antenna:	AeroAntenna AT575
		Receiver/software:	NordNav R-30/NordNav-Rx
		Sampling freq.:	1.63676 [MHz] (L1 carrier)
		Coordinates:	Variable (depending on the scenario)

Table 5.1: Measurement campaigns details

The *a priori* noise statistics were selected suitable for the purpose of evaluating each algorithm. These noise statistics refer to the noise covariance matrix factor q_w (see Appendix A) and the measurement noise covariance r. For each algorithm, the state vector consisted of a $n = 2$ dimensional vector with the second order derivative modeled as a white Gaussian noise sequence (i.e., $\phi^{(n)}(t) = w_\phi(t)$). The integration interval is 1 ms as the minimum predetection integral interval in a conventional GPS tracking loop.

5.2 Scenarios

Different scenarios were considered for evaluating the performance of the adaptive algorithms. Table 5.2 contains the description of each scenario. For each scenario, two representative satellites were chosen. The satellites with the highest and lowest C/N_0 at the acquisition stage were elected the representative satellites. Figure 5.1 and 5.2 illustrate the scenarios from the second measurements campaign in München.

5.3 Estimation of r

For the estimation of the measurement noise covariance r, the algorithm in [4] was implemented. Section 3.2 demonstrated the easiness for obtaining an estimate of this quantity based on the innovation sequence.
In order to compare the r estimates from this algorithm, the method for the C/N_0 estimation in [15] was considered. The estimation of the C/N_0 is obtained by computing the wide-band power (WBP_k) and the narrow-band power

Figure 5.1: Scenarios 1-4

Figure 5.2: Scenario 5

(NBP_k) from the I and Q arms over M samples as:

$$C/N_0 = 10 \log_{10} \left(\frac{1}{T_i} \frac{\hat{\mu}_{\mathrm{NP}} - 1}{M - \hat{\mu}_{\mathrm{NP}}} \right) \tag{5.1}$$

where

$$\hat{\mu}_{\mathrm{NP}} = \frac{1}{K} \sum_{k=1}^{K} \mathrm{NP}_k \tag{5.2}$$

	Scenario	Description
Static measurements (static receiver)	gnd	Ground station at Flughafen Innsbruck-Kranebitten (INN). Representative satellites: PRN06/PRN21
	scen1	Receiver situated under a tree. Strong absorption and scattering. Representative satellites: PRN08/PRN26
	scen2	Receiver situated in the middle of a wide flat field (in front of the Alte Pinakothek, München). Good LOS. Representative satellites: PRN18/PRN26
	scen4	Standing pedestrian by the facade of the Alte Pinakothek, München. Strong multipath. Representative satellites: PRN12/PRN26
Dynamic measurements	acft	Antenna on the roof of a Beechcraft King Air 350. En-route flight between Flughafen Braunschweig-Wolfsburg (BWE) and Flughafen Innsbruck-Kranebitten (INN) (28.000 ft altitude). Representative satellites: PRN06/PRN21
	scen3	Walking pedestrian. Moderate dynamics with good LOS. Representative satellites: PRN18/PRN26
	scen5	Bicycle ride. High dynamics with sudden satellite shadowing. Representative satellites: PRN09/PRN26

Table 5.2: Scenarios

i.e., the mean of the normalized power (NP_k) defined as:

$$\mathrm{NP}_k = \frac{\mathrm{NBP}_k}{\mathrm{WBP}_k} = \frac{\left(\sum_{i=1}^{M} I_i\right)_k^2 + \left(\sum_{i=1}^{M} Q_i\right)_k^2}{\left(\sum_{i=1}^{M} (I_i^2 + Q_i^2)\right)_k} \tag{5.3}$$

For this implementation, the wide-band power and narrow-band power was considered and averaged within a 20 ms interval ($M = 20$, $K = 20$).
Furthermore, in the range of C/N_0 (30-55 dB-Hz), the tracking error variance (i.e., the measurement noise variance) can be approximated by [15]:

$$r = \frac{1}{2C/N_0 T_i}\left(1 + \frac{1}{2C/N_0 T_i}\right) \tag{5.4}$$

Therefore, once an estimate of r was obtained using the adaptive algorithm, the estimated C/N_0 for it was obtained using (5.4).

5.3.1 Noise statistics initialization

The *a priori* measurement noise variance was set to the largest value for which Eq. (5.4) is still valid with less than 1 dB error [15] ($C/N_0 = 30$ dB-Hz). By doing this, the initialization was assured to be wrong. Regarding the process noise variance q_w, there is no intuitive value and it was set to 1000 $\mathrm{rad}^2/\mathrm{s}^3$.

5.3.2 Results

Figure 5.3 and Figure 5.4 show the C/N_0 estimation from [4] and from the algorithm in [15] for the scenarios scen2 and scen3, respectively. These two

scenarios contain the same representative satellites (PRN18 with a low C/N_0 and PRN26 with a high C/N_0), but the former is a static recording while the second is a pedestrian walk. The sample size of the innovation sequence is 750 (0.75 s). Figure 5.3 shows that the algorithm provides an estimate of r similar to that from the C/N_0 for high C/N_0 signals and a static receiver. From Figure 5.4, the algorithm still performs close to the C/N_0 estimates even for a low C/N_0.

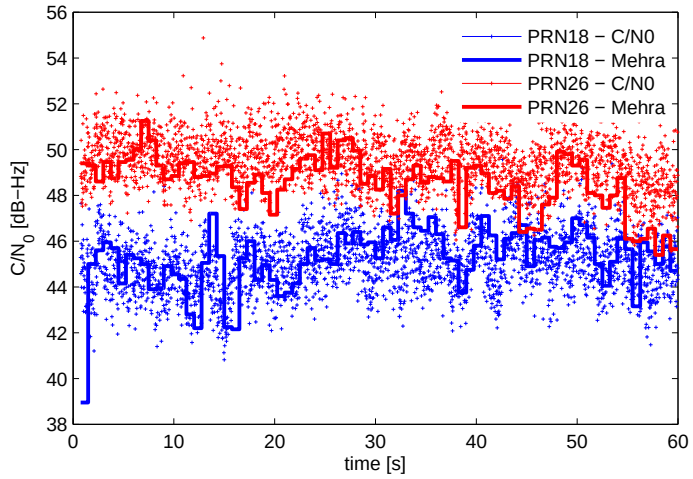

Figure 5.3: C/N_0 estimates obtained from the algorithm in [4] and [15] for the scenario scen2

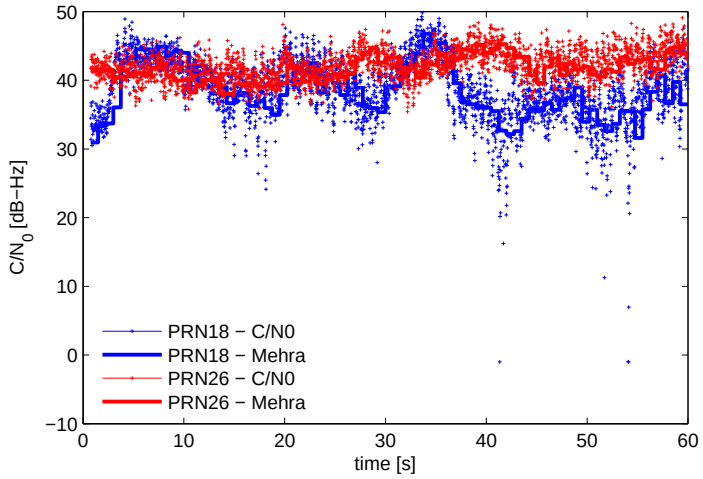

Figure 5.4: C/N_0 estimates obtained from the algorithm in [4] and [15] for the scenario scen3

5.4 Estimation of q_w and r

The estimation of the process noise variance q_w and the measurement noise variance r is based on the algorithm in [9]. The particular derivation for a $n = 2$-dimensional state vector is in Appendix B. For a Kalman filter-based PLL architecture, this derivation is also valid.
For evaluating this algorithm, it has been considered the following cases:

- Innovation sample size of 750 samples with 10 and 25 correlation lags.
- Innovation sample size of 1500 samples with 10 and 25 correlation lags.

5.4.1 Noise statistics initialization

As previously, the *a priori* measurement noise variance was set to the largest value for which Eq. (5.4) is still valid ($C/N_0 = 30$ dB-Hz). The process noise variance q_w value is 1000 rad^2/s^3 in all cases.

5.4.2 Results

Due to the large quantity of scenarios and cases considered, it has been selected the most repetitive and representative results that have been observed from all the results. This section compares the variance estimates for some scenarios and different signal strength. Of course, the purpose of a phase tracking loop is to keep the phase error as minimum as possible and then it should be observed a zero-mean noise-like discriminator output (refer to Eq. (4.11)). Nevertheless, the discriminator output is not a good measure of the performance of a Kalman filter-based tracking architecture because the magnitude of the measurement noise variance is large compared to the phase error magnitude and the effect of the discriminator noise shadows completely the phase error.
Figure 5.5 and 5.6 show the variance estimates of q_w and r for the different sample sizes N and correlation lags l for the scenarios gnd and scen2 (for the high C/N_0 signal), respectively. The similarity between scenarios (see Table 5.2) is also seen in the magnitude of the estimates of q_w and r. Moreover, it can be seen that there is no improvement for any component in $\hat{\boldsymbol{\alpha}}$ when the correlation lag l is increased. By contrast, when the sample size N is 1500, the estimate of q_w is smoothed in comparison with $N = 750$ at each adaptation stage. The discontinuities in the estimates are due to negative values. Figure 5.7 show the variance estimates for the dynamic scenario scen3 and the high C/N_0 signal (PRN26). It is interesting to note that the dynamics of the scenario are reflected in larger values of the q_w and r when compared to the previous scenario scen2. Figure 5.8 illustrates for the same scenario scen3 the variance estimates of the low C/N_0 signal (PRN18). Comparing Figs. 5.7 and 5.8, it is clear the difference in the carrier-to-noise ratio between signals according to the variance estimates.
Similarly, Figures 5.9 and 5.10 show the same variance quantities for the dynamic scenario acft. Finally, Figures 5.11 and 5.12 plot the same quantities for the scenario scen5. In this case, the sudden shadowing can be also seen in the large magnitude of the variances.

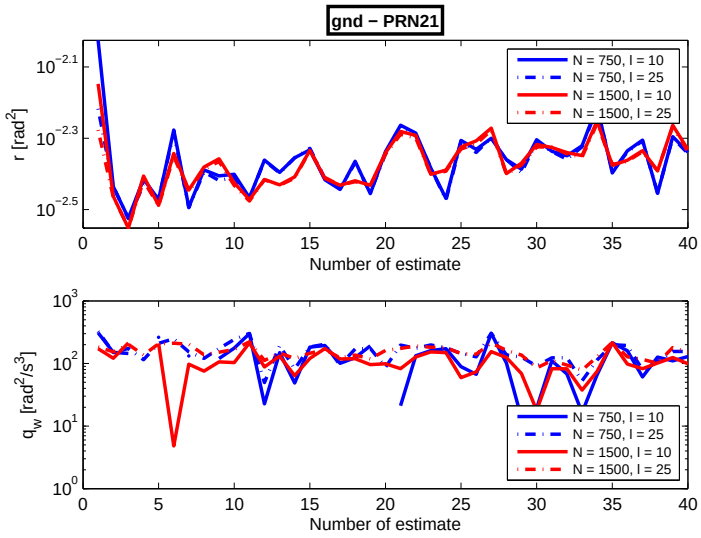

Figure 5.5: q_w and r estimates obtained from the algorithm in [9] for different sample sizes N and correlation lags l and for the scenario gnd (PRN21)

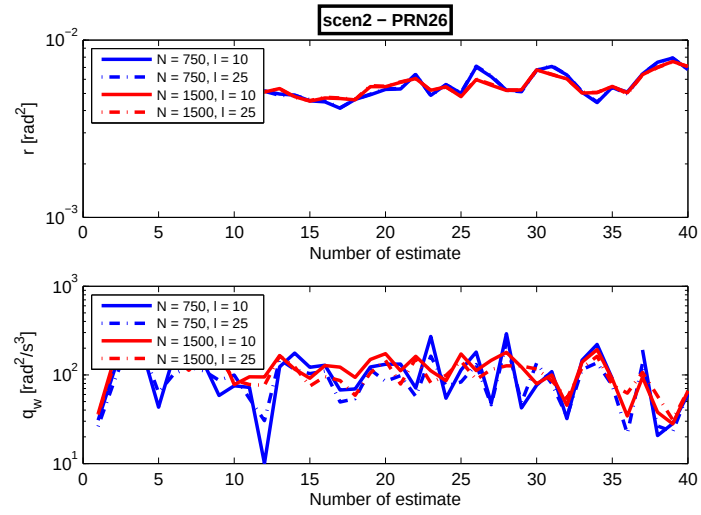

Figure 5.6: q_w and r estimates obtained from the algorithm in [9] for different sample sizes N and correlation lags l and for the scenario scen2 (PRN26)

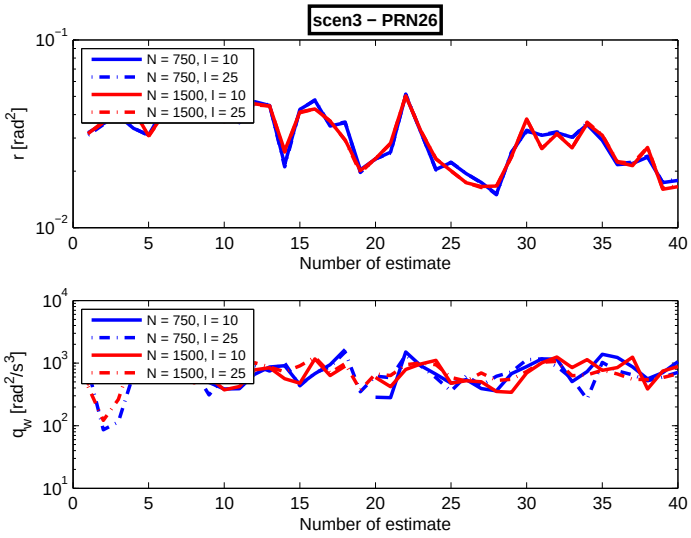

Figure 5.7: q_w and r estimates obtained from the algorithm in [9] for different sample sizes N and correlation lags l and for the scenario scen3 (PRN26)

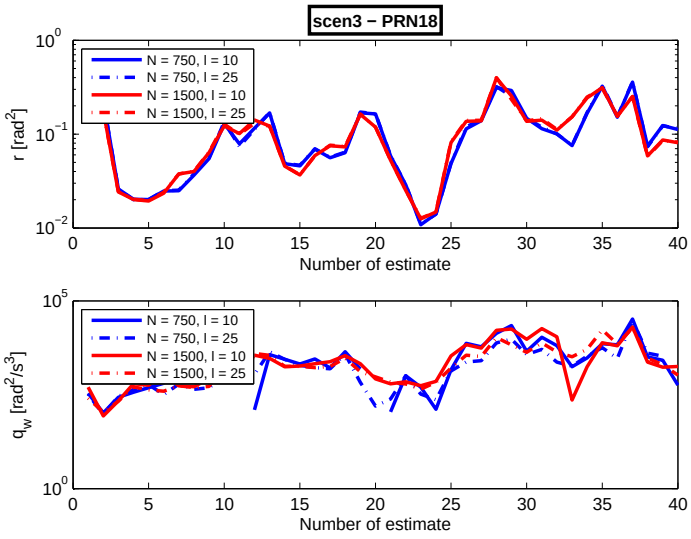

Figure 5.8: q_w and r estimates obtained from the algorithm in [9] for different sample sizes N and correlation lags l and for the scenario scen3 (PRN18)

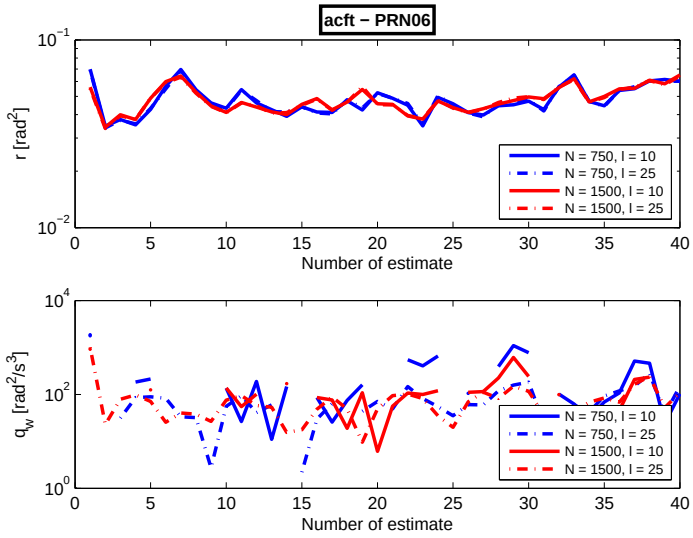

Figure 5.9: q_w and r estimates obtained from the algorithm in [9] for different sample sizes N and correlation lags l and for the scenario acft (PRN06)

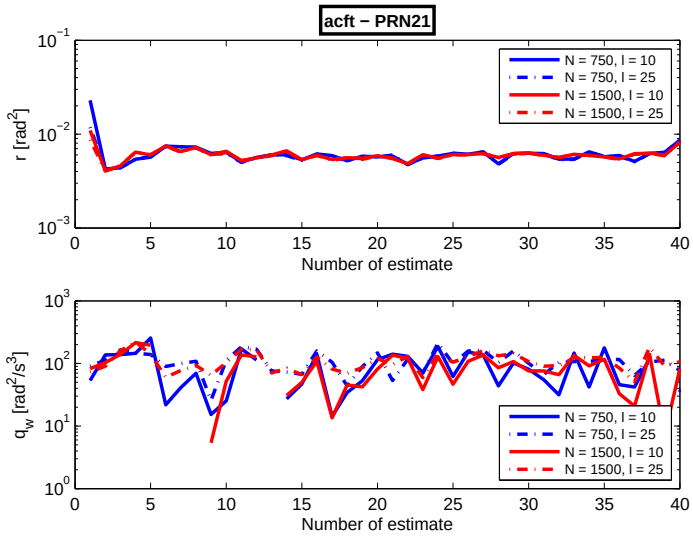

Figure 5.10: q_w and r estimates obtained from the algorithm in [9] for different sample sizes N and correlation lags l and for the scenario acft (PRN21)

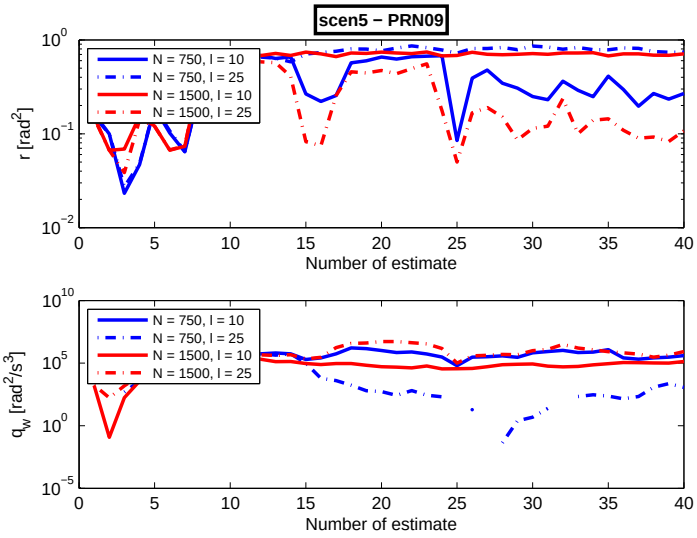

Figure 5.11: q_w and r estimates obtained from the algorithm in [9] for different sample sizes N and correlation lags l and for the scenario scen5 (PRN09)

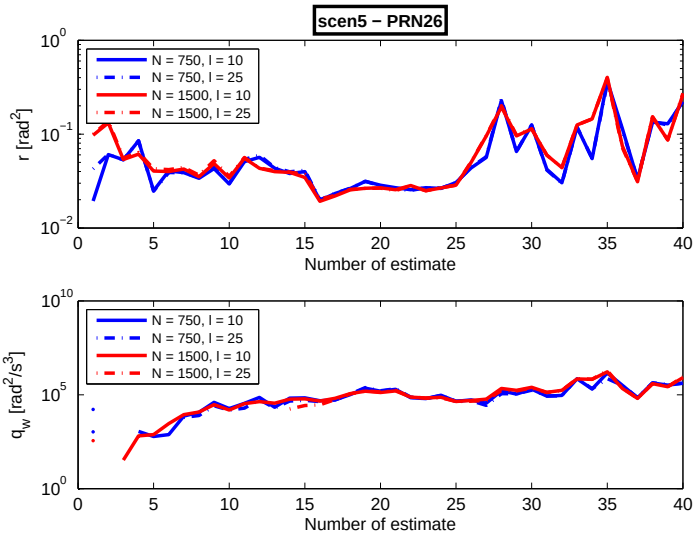

Figure 5.12: q_w and r estimates obtained from the algorithm in [9] for different sample sizes N and correlation lags l and for the scenario scen5 (PRN26)

Chapter 6

Conclusions

Chapter 2 has shown the effects of a wrong noise statistics initialization and a dimension mismatch between the actual state vector and the state estimate vector for different simulated trajectories and estimation processes. The availability of the actual state vector made it possible to compare the actual error covariance matrix to the estimated by the Kalman filter.
For a wrong process noise initialization, the error variance of the first state estimate vector component out of the Kalman filter was slightly greater with respect to the actual error variance when a larger scaled version of the process noise covariance matrix than the actual was used ($q > 1$). Moreover, the performance of the Kalman filter is suboptimally for any wrong process noise covariance.
Similarly, a wrong measurement noise would lead to the same suboptimal filter performance and a larger error variance in the estimates even for a correct process noise covariance initialization. Nevertheless, a measure of this value can be obtained in a GNSS tracking architecture using the carrier-to-noise ratio C/N_0.
As shown in Figs. 2.2 and 2.4, an initialization for a large scaled version of the process noise covariance matrix would result in a better performance of the Kalman filter and smaller estimation errors. Moreover, the effect of a different dimension between the simulated trajectory and the state estimate vector is also translated into large estimation errors because the process noise covariance matrix would look very different for each dimension considered.
Some innovation based adaptive algorithms were implemented and evaluated in Chapter 3 for a simulated trajectory and in Chapter 5 for a Kalman filter-based tracking architecture. These methods consider a finite sample size of the innovation sequence $\boldsymbol{\nu}_k$ and the biased autocorrelation function of it. The estimation of the measurement noise covariance $\mathbf{R}$ is straightforward when using any of these methods. By contrast, the estimation of the process noise covariance matrix $\mathbf{Q}$ is not reliable and consistent when using these innovation correlation methods but for the algorithm in [9]. The reason would be probably that this last algorithm considers more than 2 lags in the computation of the innovation autocorrelation function for each N samples rather than just correlate once all the sequence. Therefore, the fact of considering l lags through a N-length innovation sequence when calculating the autocorrelation function seems to provide more information. Similarly, the direct estimation of the optimum gain was not a reliable method. The reason would be in the white-like spectrum of an innovation sequence even for a wrong noise statistics.

Finally, a numerical indication of the process noise variance q_w was obtained from the algorithm in [9] for a Kalman-filter carrier-phase tracking architecture. Different scenarios were considered with different and common signal dynamics and strength.

6.1 Future work

From this conclusion, it is suggested a new study of each algorithm based on reproducible and known signal and constellation dynamics. This work has dealt only with real GPS measurements in an urban environment and limited receiver characteristics. Therefore, a more extensive reproducibility is necessary.
Moreover, the algorithm in [9] needs a large computation time and effort. An efficient similar version of this algorithm has also presented in [16], but it has not been considered. Thus another step would be the reimplementation of the algorithm in a more efficient way.
Finally, the benefit of using an adaptive algorithm in the tracking accuracy is necessary to be checked. Obviously, the effect of these adaptive techniques can be seen upon the error covariance matrix and for that reason it would be interesting to observe this quantity.

Appendix A

Trajectory (Phase) Model

Through this work, the n-th order derivative of the phase $\phi(t)$ is modeled as a white Gaussian noise sequence (i.e., $\phi^{(n)}(t) = w_\phi(t)$). According to Taylor's theorem, $\phi(t)$ can be time-expanded according to [13]:

$$\phi(t+T_i) = \sum_{j=0}^{n-1} \phi^{(j)}(t)\frac{T_i^j}{j!} + R_n(t, t+T_i, n) \tag{A.1}$$

where the remainder R_l is defined as:

$$R_l(t_1, t_2, l) = \int_{t_1}^{t_2} w_\phi(u)\frac{(t_2-u)^{l-1}}{(l-1)!}du \tag{A.2}$$

Carrying this expansion on the higher derivatives of $\phi(t)$, the resulting vector-form of the phase model is:

$$\underbrace{\begin{bmatrix} \phi^{(0)}(t_{k+1}) \\ \vdots \\ \phi^{(n-1)}(t_{k+1}) \end{bmatrix}}_{\mathbf{x}(t_{k+1})} = \mathbf{A}_n\mathbf{x}(t_k) + \underbrace{\begin{bmatrix} R_n(t_k, t_{k+1}, n) \\ \vdots \\ R_1(t_k, t_{k+1}, 1) \end{bmatrix}}_{\mathbf{w}_\phi(t_k)} \tag{A.3}$$

with

$$(\mathbf{A}_n)_{h,j} = \begin{cases} \dfrac{T_i^{j-h}}{(j-h)!}, & \text{if } j-h \geq 0 \\ 0 & \text{otherwise} \end{cases} \tag{A.4}$$

and $T_k = t_{k+1} - t_k$ For the particular case of $n = 2$, the covariance matrix associated with the noise sequences $\mathbf{w}_\phi(t)$ is defined as:

$$\mathbb{E}\left\{\mathbf{w}_\phi(t_i)\mathbf{w}_\phi(t_j)^T\right\} = \mathbb{E}\left\{\begin{bmatrix} R_2(t_i, t_{i+1}, 2) \\ R_1(t_i, t_{i+1}, 1) \end{bmatrix}\begin{bmatrix} R_2(t_j, t_{j+1}, 2) & R_1(t_j, t_{j+1}, 1) \end{bmatrix}\right\} \tag{A.5}$$

Substituting in Eq. (A.5) the corresponding expression of each remainder:

$$\mathbb{E}\left\{\mathbf{w}_\phi(t_i)\mathbf{w}_\phi(t_j)^T\right\} = \begin{cases} \mathbf{Q} & \text{if } i = j \\ 0 & \text{otherwise} \end{cases} \tag{A.6}$$

where

$$\mathbf{Q} = q_w \begin{bmatrix} \frac{T_i^3}{3} & \frac{T_i^2}{2} \\ \frac{T_i^2}{2} & T_i \end{bmatrix} \tag{A.7}$$

and q_w is the measurement noise variance in units of rad^2/s^3.

A.1 Measurement model

Similarly, the phase measurement model is defined in discrete-time as:

$$\mathbf{y}_k = \mathbf{C}_n \mathbf{x}_k + \mathbf{v}_k \tag{A.8}$$

where

$$\mathbf{C}_n = \begin{bmatrix} 1 & \frac{T_i}{2} & \cdots & \frac{T_i^n}{n!} \end{bmatrix} \tag{A.9}$$

is defined as the observation or measurement mapping matrix and $\mathbf{v}_k$ is the measurement noise vector with covariance matrix $\mathbf{R}$, i.e.:

$$\mathbb{E}\left\{\mathbf{v}_i {\mathbf{v}_j}^T\right\} = \begin{cases} \mathbf{R} & \text{if } i = j \\ 0 & \text{otherwise} \end{cases} \tag{A.10}$$

Appendix B

Bélanger's Algorithm Derivation

This appendix derives the algorithm in [9] for the particular case of a $n = 2$-dimensional state vector. This method states that if the covariance matrices are linear in a set of parameters, then the correlation function of the innovation sequence is also a linear function of this set of parameters. Therefore, $\mathbf{Q}$ and $\mathbf{R}$ are regarded as linear functions of the $M = 2$ components of a vector $\boldsymbol{\alpha}$, i.e.:

$$\begin{aligned} \mathbf{R} &= \alpha_1; \\ \mathbf{Q} &= \alpha_2 \mathbf{Q}_0 \end{aligned} \tag{B.1}$$

For a $n = 2$-dimensional state vector and $p = 1$-dimensional measurement vector, the noise sequences $\mathbf{v}_k$ and $\mathbf{w}_k$ covariances are:

$$\mathbb{E}\left\{\mathbf{v}_i {\mathbf{v}_j}^T\right\} = \alpha_1 \mathbf{I}_p \delta_{ij} \tag{B.2}$$

$$\mathbb{E}\left\{\mathbf{w}_i {\mathbf{w}_j}^T\right\} = \alpha_2 \mathbf{Q}_0 \delta_{ij} \tag{B.3}$$

$$\mathbb{E}\left\{\mathbf{v}_i {\mathbf{w}_j}^T\right\} = \mathbf{0}_{pxn}, \quad \text{for any } i \text{ and } j \tag{B.4}$$

where $\mathbf{I}_p$ and $\mathbf{0}_{pxn}$ denote the p-dimensional identity and pxn zero matrix, respectively, and δ_{ij} is the Kronecker's delta defined as:

$$\delta_{ij} = \begin{cases} 1 & \text{if } i = j \\ 0 & \text{otherwise} \end{cases} \tag{B.5}$$

Let's define:

$$\mathbf{e}_k = \mathbf{x}_k - \hat{\mathbf{x}}_k \tag{B.6}$$

Substituting Eqs. (2.1), (2.2) and (2.10) in (B.6):

$$\mathbf{e}_{k+1} = \underbrace{(\mathbf{I} - \mathbf{KC})\mathbf{A}}_{\boldsymbol{\Phi}} \mathbf{e}_k + \underbrace{(\mathbf{I} - \mathbf{KC})}_{\boldsymbol{\theta}} \mathbf{w}_k - \mathbf{K}\mathbf{v}_{k+1} \tag{B.7}$$

More generally,

$$\mathbf{e}_k = \sum_{j=0}^{k-1} \boldsymbol{\Phi}^{k-j-1} \left(\boldsymbol{\theta}\mathbf{w}_j - \mathbf{K}\mathbf{v}_{j+1}\right) \tag{B.8}$$

where it is assumed a perfect initialization, i.e., $\mathbf{e}_0 = \mathbf{0}$. An alternative expression for the innovation sequence in Eq. (3.1) is:

$$\begin{aligned}\boldsymbol{\nu}_k = \mathbf{y}_k - \mathbf{C}\hat{\mathbf{x}}_k^- =& \mathbf{C}\mathbf{x}_k + \mathbf{v}_k - \mathbf{C}\mathbf{A}\hat{\mathbf{x}}_{k-1} \\ =& \mathbf{C}(\mathbf{A}\mathbf{x}_{k-1} + \mathbf{w}_{k-1}) + \mathbf{v}_k - \mathbf{C}\mathbf{A}\hat{\mathbf{x}}_{k-1} \\ =& \mathbf{C}\mathbf{A}\mathbf{e}_{k-1} + \mathbf{C}\mathbf{w}_{k-1} + \mathbf{v}_k \\ =& \mathbf{C}\mathbf{A}\sum_{j=0}^{k-2}\boldsymbol{\Phi}^{k-j-2}\left(\boldsymbol{\theta}\mathbf{w}_j - \mathbf{K}\mathbf{v}_{j+1}\right) + \mathbf{C}\mathbf{w}_{k-1} + \mathbf{v}_k \end{aligned} \quad \text{(B.9)}$$

Therefore,

$$\begin{aligned}\mathbb{E}\left\{\boldsymbol{\nu}_k\boldsymbol{\nu}_{k-l}^T\right\} = \mathbb{E}\Bigg\{ & \left[\mathbf{C}\mathbf{A}\sum_{j=0}^{k-2}\boldsymbol{\Phi}^{k-j-2}\left(\boldsymbol{\theta}\mathbf{w}_j - \mathbf{K}\mathbf{v}_{j+1}\right) + \mathbf{C}\mathbf{w}_{k-1} + \mathbf{v}_k\right] \\ & \left[\mathbf{C}\mathbf{A}\sum_{i=0}^{k-l-2}\boldsymbol{\Phi}^{k-l-i-2}\left(\boldsymbol{\theta}\mathbf{w}_i - \mathbf{K}\mathbf{v}_{i+1}\right) + \mathbf{C}\mathbf{w}_{k-l-1} + \mathbf{v}_{k-l}\right]^T\Bigg\}\end{aligned} \quad \text{(B.10)}$$

The expression in (B.10) should be evaluated for each term separately as follows:

$$\begin{aligned}\mathbb{E}\left\{\boldsymbol{\nu}_k\boldsymbol{\nu}_{k-l}^T\right\} =& \mathbb{E}\left\{\mathbf{C}\mathbf{A}\sum_{j=0}^{k-2}\boldsymbol{\Phi}^{k-j-2}\boldsymbol{\theta}\mathbf{w}_j\sum_{i=0}^{k-l-2}\mathbf{w}_i^T\boldsymbol{\theta}^T\left(\boldsymbol{\Phi}^T\right)^{k-l-i-2}\mathbf{A}^T\mathbf{C}^T\right\} \\ &+ \mathbb{E}\left\{\mathbf{C}\mathbf{A}\sum_{j=0}^{k-2}\boldsymbol{\Phi}^{k-j-2}\boldsymbol{\theta}\mathbf{w}_j\mathbf{w}_{k-l-1}^T\mathbf{C}^T\right\} \\ &+ \mathbb{E}\left\{\mathbf{C}\mathbf{A}\sum_{j=0}^{k-2}\boldsymbol{\Phi}^{k-j-2}\mathbf{K}\mathbf{v}_{j+1}\sum_{i=0}^{k-l-2}\mathbf{v}_{i+1}^T\mathbf{K}^T\left(\boldsymbol{\Phi}^T\right)^{k-l-i-2}\mathbf{A}^T\mathbf{C}^T\right\} \\ &- \mathbb{E}\left\{\mathbf{C}\mathbf{A}\sum_{j=0}^{k-2}\boldsymbol{\Phi}^{k-j-2}\mathbf{K}\mathbf{v}_{j+1}\mathbf{v}_{k-l}^T\right\} \\ &+ \mathbb{E}\left\{\mathbf{C}\mathbf{w}_{k-1}\mathbf{w}_{k-l-1}^T\mathbf{C}^T\right\} + \mathbb{E}\left\{\mathbf{v}_k\mathbf{v}_{k-l}^T\right\}\end{aligned} \quad \text{(B.11)}$$

Given (B.2) and (B.3), Equation (B.11) reduces for $l \geq 0$ to:

$$\begin{aligned}\mathbb{E}\left\{\boldsymbol{\nu}_k\boldsymbol{\nu}_{k-l}^T\right\} =& \alpha_2\sum_{j=0}^{k-l-2}\mathbf{C}\mathbf{A}\boldsymbol{\Phi}^{k-j-2}\boldsymbol{\theta}\mathbf{Q}_0\boldsymbol{\theta}^T\left(\boldsymbol{\Phi}^T\right)^{k-l-j-2}\mathbf{A}^T\mathbf{C}^T \\ &+ \alpha_2\mathbf{C}\mathbf{A}\boldsymbol{\Phi}^{l-1}\boldsymbol{\theta}\mathbf{Q}_0\mathbf{C}^T \\ &+ \alpha_1\sum_{j=0}^{k-l-2}\mathbf{C}\mathbf{A}\boldsymbol{\Phi}^{k-j-2}\mathbf{K}\mathbf{K}^T\left(\boldsymbol{\Phi}^T\right)^{k-l-j-2}\mathbf{A}^T\mathbf{C}^T \\ &- \alpha_1\mathbf{C}\mathbf{A}\boldsymbol{\Phi}^{l-1}\mathbf{K}u(l-1) \\ &+ \alpha_2\mathbf{C}\mathbf{Q}_0\mathbf{C}^T\delta(l) + \alpha_1\delta(l)\end{aligned} \quad \text{(B.12)}$$

where $\delta(j)$ is the Dirac delta defined as:

$$\delta(j) = \begin{cases}1 & \text{if } j = 0 \\ 0 & \text{otherwise}\end{cases} \quad \text{(B.13)}$$

and $u(l-1)$ is the Heaviside (unit-step) function:

$$u(t) = \begin{cases} 1 & \text{if } t \geq 0 \\ 0 & \text{otherwise} \end{cases} \tag{B.14}$$

For $k = 1, \ldots, N$ and $l = 0, \ldots, L$, the resulting set of equations is:

$$\boldsymbol{\sigma}(k,l) = \mathcal{F}\boldsymbol{\alpha} + \boldsymbol{\eta}_{k,l} \tag{B.15}$$

where

$$\boldsymbol{\sigma}(k,l) = \begin{bmatrix} \boldsymbol{\nu}_k \boldsymbol{\nu}_{k-L} \\ \vdots \\ \boldsymbol{\nu}_k \boldsymbol{\nu}_k \\ \vdots \\ \boldsymbol{\nu}_N \boldsymbol{\nu}_{N-L} \\ \vdots \\ \boldsymbol{\nu}_N \boldsymbol{\nu}_N \end{bmatrix} \tag{B.16}$$

Therefore, the least-squares solution is given by:

$$\hat{\boldsymbol{\alpha}} = \left[\mathcal{F}^T \mathbf{W}^{-1} \mathcal{F}\right]^{-1} \mathcal{F}^T \mathbf{W}^{-1} \boldsymbol{\sigma}(k,l) \tag{B.17}$$

where the weighting matrix $\mathbf{W}$ is defined as $\mathbf{W}^{-1} \equiv \mathbb{E}\left[\boldsymbol{\eta}_{k,l} \boldsymbol{\eta}_{k,l}^T\right]$, i.e., the covariance matrix of $\boldsymbol{\eta}_{k,l}$. In all simulations, the weighted least-squares showed almost the same results as with the unweighted least-squares solution. Therefore the derivation of the weighting matrix is omitted here and the reader is referred to [9] for more details.
The algorithm from Bélanger differs from the other innovation correlation methods in the fact that $l = 0, \cdots, L$ lags are considered for a innovation sequence of length N (i.e., the vector $\boldsymbol{\sigma}(k,l)$). Therefore, the innovation sequence is analyzed in more detail and more information is extracted. Of course, this procedure requires a large time-consuming computation.

Bibliography

[1] R. Mehra, "Approaches to adaptive filtering," *IEEE Transactions on Automatic Control*, vol. 17, no. 5, pp. 693–698, October 1972.

[2] M. Braasch and A. van Dierendonck, "GPS receiver architectures and measurements," *Proceedings of the IEEE*, vol. 87, no. 1, pp. 48–64, January 1999.

[3] M. S. Grewal and A. P. Andrews, *Kalman Filtering : Theory and Practice Using MATLAB*, 2nd ed. Wiley-Interscience, January 2001.

[4] R. Mehra, "On the identification of variances and adaptive Kalman filtering," *Automatic Control, IEEE Transactions on*, vol. 15, no. 2, pp. 175–184, April 1970.

[5] G. M. Jenkins and D. G. Watts, *Spectral analysis and its applications*. San Francisco: Holden-Day, 1968.

[6] G. M. Ljung and G. E. P. Box, "On a measure of lack of fit in time series models," *Biometrika*, vol. 65, no. 2, pp. 297–303, 1978.

[7] K. A. Myers and B. D. Tapley, "Adaptive sequential estimation with unknown noise statistics," *IEEE Transactions on Automatic Control*, vol. 21, no. 4, pp. 520–523, August 1976.

[8] P. S. Maybeck, *Stochastic models, estimation, and control*. Academic Press, 1982, vol. Volume 2.

[9] P. R. Bélanger, "Estimation of noise covariance matrices for a linear time-varying stochastic process," *Automatica*, vol. 10, no. 3, pp. 267–275, 1974.

[10] B. Carew and P. Bélanger, "Identification of optimum filter steady-state gain for systems with unknown noise covariances," *IEEE Transactions on Automatic Control*, vol. 18, no. 6, pp. 582–587, 1973.

[11] K. Borre, D. M. Akos, N. Bertelsen, P. Rinder, and S. H. Jensen, *A Software-Defined GPS and Galileo Receiver*, ser. Applied Numerical Harmonic Analysis. Birkhäuser Boston, 2007.

[12] C. O'Driscoll and G. Lachapelle, "Comparison of traditional and Kalman filter based tracking architectures," in *Proceedings of the European Navigation Conference ENC – GNSS 2009*, Naples, May 2009.

[13] K. Giger, P. Henkel, and C. Günther, "Joint satellite code and carrier tracking," in *ION Internationl Technical Meeting*, San Diego, January 2010.

[14] B. W. Parkinson and J. J. S. Jr., *Global Positioning System: Theory and Applications*. Progress in Astronautics and Aeronautics, 1996, vol. Volume I.

[15] A. J. Van Dierendonck, "GPS receivers," in *Global Positioning System: Theory and Application*, B. W.Parkinson and J. J. Spilker, Eds., vol. I. American Institute of Aeronautics and Astronautics (AIAA), 1996, pp. 329–407.

[16] D. Dee, S. Cohn, A. Dalcher, and M. Ghil, "An efficient algorithm for estimating noise covariances in distributed systems," *Automatic Control, IEEE Transactions on*, vol. 30, no. 11, pp. 1057 – 1065, nov 1985.

[17] R. G. Brown and P. Y. C. Hwang, *Introduction to Random Signals and Applied Kalman Filtering*. John Wiley & Sons, Inc., 1992.

[18] A. Papoulis and S. U. Pillai, *Probability, Random Variables, and Stochastic Processes*, fourth edition ed. McGraw-Hill, 2002.

[19] A. H. Mohamed and K. P. Schwarz, "Adaptive kalman filtering for INS/GPS," *Journal of Geodesy*, vol. 73, no. 4, pp. 193–203, May 1999.

[20] M. Haugh, *The Monte Carlo Framework, Examples from Finance and Generating Correlated Random Variables*. University of Columbia, 2004.